RESEARCH ARTICLE

Key Points:
- Boron-isotope-based pH reconstructions indicate that the subtropical/subpolar Southwest Pacific was a source of CO_2 during the last 19 ka
- Major CO_2 outgassing from the Southwest Pacific was associated with enhanced ventilation of intermediate waters between 16.5 and 14 kyr BP
- A surface pH/pCO_2 composite derived from 12 planktic $\delta^{11}B$ records shows widespread CO_2 release from the ocean during the last deglaciation

Supporting Information:
- Supporting Information S1
- Figure S1
- Figure S2
- Figure S3
- Figure S4
- Figure S5
- Figure S6
- Figure S7
- Figure S8
- Figure S9
- Figure S10

Correspondence to:
J. Shao,
junshao@usc.edu

Atmosphere-Ocean CO₂ Exchange Across the Last Deglaciation From the Boron Isotope Proxy

Jun Shao[1] (ID), **Lowell D. Stott[1]** (ID), **William R. Gray[2,3]** (ID), **Rosanna Greenop[2]** (ID), **Ingo Pecher[4]** (ID), **Helen L. Neil[5]**, **Richard B. Coffin[6]**, **Bryan Davy[7]** (ID), and **James W.B. Rae[2]** (ID)

[1]Department of Earth Science, University of Southern California, Los Angeles, CA, USA, [2]School of Earth and Environmental Sciences, University of St Andrews, St Andrews, UK, [3]Laboratoire des Sciences du Climat et de l'Environnement (LSCE/IPSL), Gif-sur-Yvette, France, [4]School of Environment, University of Auckland, Auckland, New Zealand, [5]Department of Marine Geology, The National Institute of Water and Atmospheric Research, Auckland, New Zealand, [6]Department of Physical and Environmental Sciences, Texas A&M University, Corpus Christi, TX, USA, [7]Department of Marine Geosciences, GNS Science, Lower Hutt, New Zealand

Abstract Identifying processes within the Earth System that have modulated atmospheric pCO_2 during each glacial cycle of the late Pleistocene stands as one of the grand challenges in climate science. The growing array of surface ocean pH estimates from the boron isotope proxy across the last glacial termination may reveal regions of the ocean that influenced the timing and magnitude of pCO_2 rise. Here we present two new boron isotope records from the subtropical-subpolar transition zone of the Southwest Pacific that span the last 20 kyr, as well as new radiocarbon data from the same cores. The new data suggest this region was a source of carbon to the atmosphere rather than a moderate sink as it is today. Significantly higher outgassing is observed between ~16.5 and 14 kyr BP, associated with increasing $\delta^{13}C$ and $[CO_3]^{2-}$ at depth, suggesting loss of carbon from the intermediate ocean to the atmosphere. We use these new boron isotope records together with existing records to build a composite pH/pCO_2 curve for the surface oceans. The pH disequilibrium/CO_2 outgassing was widespread throughout the last deglaciation, likely explained by upwelling of CO_2 from the deep/intermediate ocean. During the Holocene, a smaller outgassing peak is observed at a time of relatively stable atmospheric CO_2, which may be explained by regrowth of the terrestrial biosphere countering ocean CO_2 release. Our stack is likely biased toward upwelling/CO_2 source regions. Nevertheless, the composite pCO_2 curve provides robust evidence that various parts of the ocean were releasing CO_2 to the atmosphere over the last 25 kyr.

1. Introduction

Growth and retreat of ice sheets in the late Pleistocene was accompanied by variations in atmospheric pCO_2 from ~180 ppm during the glacial maxima to 280 ppm during peak preindustrial interglacials (Petit et al., 1999). Most explanations for this CO_2 change have focused on a more efficient polar-ocean biological pump, driven by a combination of increased stratification (Basak et al., 2018; Ferrari et al., 2014; Franois et al., 1997) and stronger iron fertilization in the Southern Ocean (Martinez-Garcia et al., 2014). Reduced hydrothermal flux of CO_2 has also recently been suggested to play a role (Lund et al., 2016; Stott & Timmermann, 2011). However, the relative importance and timing of the mechanisms that contributed to glacial CO_2 change is yet to be fully resolved.

To improve constraints on the role of ocean-atmosphere CO_2 exchange between the ocean and the atmosphere in glacial-interglacial changes in atmospheric pCO_2, several recent studies have examined when and where CO_2 was entering and leaving the ocean using sea surface carbonate chemistry reconstructions. Changes in surface CO_2 chemistry may be driven by changes in upwelling or stratification and changes in the biological soft tissue and $CaCO_3$ pumps. In turn these influence CO_2 gas exchange, which is determined by the CO_2 partial pressure gradient between the surface ocean and the atmosphere (ΔpCO_2) and the gas exchange coefficient, which is affected by wind speed. Tracking past air-sea CO_2 exchange may help test hypotheses that have been put forward to explain glacial/interglacial atmospheric pCO_2 variability.

The boron isotope composition ($\delta^{11}B$) of foraminifera is a proxy for oceanic pH (Foster & Rae, 2016; Hemming & Hanson, 1992; Hönisch & Hemming, 2005). This proxy is based on the pH dependency of

boron speciation in seawater between boric acid (B (OH)$_3$) and borate ion (B (OH)$_4^-$) (Dickson, 1990). At low pH (< ~8.6), seawater boron primarily exists in the form of boric acid, whereas at high pH (> ~8.6), seawater boron is dominantly present in the form of borate. Because there is a constant equilibrium fractionation of 27.2‰ associated with this speciation (Klochko et al., 2006), the boron isotopic composition of each species is also pH dependent. A positive correlation between the boron isotope composition of planktic foraminifera and pH has been established through culturing experiments (Henehan et al., 2013; Sanyal et al., 1996, 2001). However, the δ^{11}B in calcite from various foraminiferal species deviates from that of the borate in seawater to varying degrees. This may arise from biological processes, including respiration and photosynthesis that are collectively referred to as "vital effects" (Hönisch et al., 2003; Rae, 2018; Zeebe et al., 2003). As a result, species-specific calibrations have been developed from culturing experiments, sediment core tops, sediment traps, and plankton tows (Henehan et al., 2013, 2016; Sanyal et al., 1996).

By taking advantage of the calibrated boron-pH proxy, a number of studies have investigated the history of ocean-atmosphere CO_2 exchange across the last deglaciation from sites in the tropical Pacific (Martínez-Botí et al., 2015; Palmer & Pearson, 2003), the North Pacific (Gray, Rae, et al., 2018), the North Indian Ocean (Naik et al., 2015; Palmer et al., 2010), the tropical Atlantic (Foster, 2008; Foster & Sexton, 2014; Henehan et al., 2013), the North Atlantic (Ezat et al., 2017; Yu et al., 2013), and the South Atlantic (Martínez-Botí et al., 2015; Figure 1a). Collectively, the available records reveal millennial-scale δ^{11}B variations that reflect substantial changes in air-sea ΔpCO_2 over the deglaciation (Figure 2). These variations have been interpreted to reflect local or regional changes in upwelling intensity, the CO_2 content of subsurface waters, and the efficiency of the biological pump. While each of these proposed mechanisms can be used to explain the individual δ^{11}B records, the collective influence of these changes on air-sea ΔpCO_2 has not been evaluated. Here, we consider the implication of the combined reconstructed anomalies on the evolution of atmospheric pCO_2.

As the number of boron isotope records has expanded to various parts of the ocean, it may now be possible to evaluate how the records reflect global and local influences. However, the subtropical and subpolar South Pacific remain poorly constrained (Figure 1a). Hence, a global picture of the air-sea exchange of CO_2 is far from complete without additional reconstructions from these areas. To address this, we present two new boron isotope reconstructions from cores recovered from Chatham Rise in the subtropical-subpolar transition zone of the SW Pacific. Although located in a moderate CO_2 sink region today, this site may also be influenced by changes in ventilation and biological pump efficiency in the Southern Ocean (Allen et al., 2015; McCave et al., 2008; Studer et al., 2015), migration of the subtropical front (Bostock et al., 2015), and/or localized inputs of radiocarbon-dead carbon (Ronge et al., 2016) on glacial-interglacial timescales. We also generate new benthic-planktic radiocarbon data to trace how reconstructed changes in CO_2 outgassing relate to changes in ventilation at depth. We combine our new boron isotope records with available records to build an initial composite sea surface pH reconstruction that spans the last 25 kyr and use this composite to assess whether the available data provide a realistic representation of global surface ocean surface CO_2 exchange. Our null hypothesis is that a composite pH/pCO_2 record that includes both source and sink regions constitutes a first-order representation of the equilibrium exchange of CO_2 between the surface ocean and atmosphere over the last 25 kyr. The null hypothesis predicts the following: First, during times of relatively stable atmospheric CO_2, the composite ocean pCO_2 stack should be roughly in equilibrium with the atmosphere; second, during intervals when the oceans released CO_2 to the atmosphere, the composite pCO_2 should be higher than the contemporary atmospheric pCO_2, with larger offsets occurring when atmospheric pCO_2 rose rapidly. Alternatively, the available records may be biased because of their locations, such that the regional ocean/atmosphere dynamics or extra carbon input from a local source overshadow the history of equilibrium exchange between the ocean and atmosphere. We test the null hypothesis in both the pH and the pCO_2 space. The boron isotope pH composite is evaluated against an independent estimation of the global mean equilibrium sea surface pH (GMSSpH), obtained by forcing the Earth System model cGENIE (Cao et al., 2009; Ridgwell et al., 2007) with the ice core record of atmospheric pCO_2 over the last 25 kyr (Bereiter et al., 2015; Monnin et al., 2001). In the model simulation, atmospheric pCO_2 data from ice cores are treated as a constraint instead of a problem to solve. We also compare the boron isotope-derived pCO_2 composite directly with the atmospheric pCO_2 record.
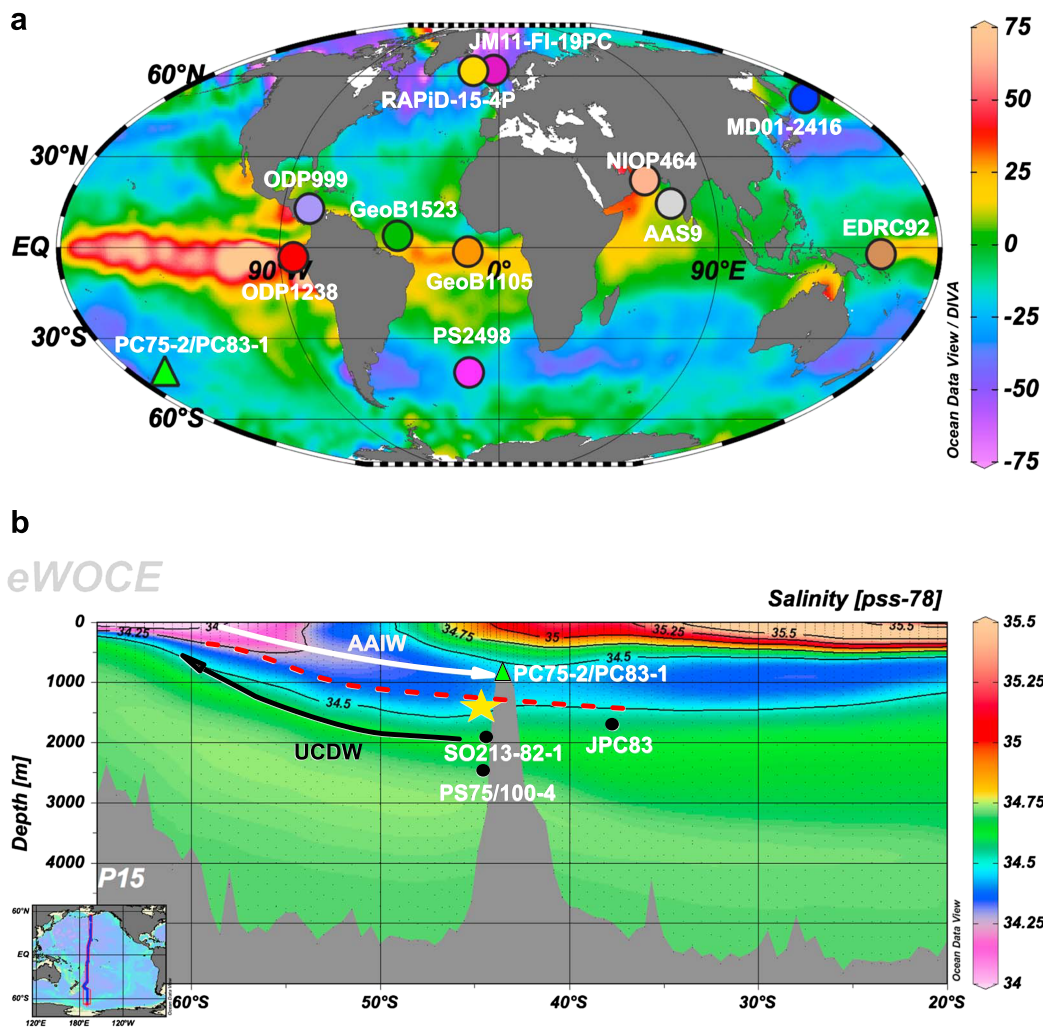
Figure 1. (a) Map of mean annual ΔpCO_2 sea air. Oceanic sinks and sources are presented by negative and positive ΔpCO_2 sea air values (Takahashi et al., 2009), respectively. The green triangle shows the location of the studied sediment cores PC75-2 and PC83-1. The circles show the locations of the cores with published boron isotope data that span the last deglaciation. (b) Salinity of the P15 transect from the World Ocean Circulation Experiment. The yellow star shows the location of corals (Hines et al., 2015); the black circles show the locations of other sediment cores (Allen et al., 2015; Ronge et al., 2016) discussed in this study. The red-dotted line marks the boundary between Antarctic Intermediate Water (AAIW) and upper circumpolar Deep Water (UCDW).

2. Methods:

2.1. Oceanographic Settings for Cores PC75-2 and PC83-1

In the SW Pacific today, the subtropical gyre between 20°S to 45°S is a carbon sink, while the surface waters south of the subtropical front (STF) between 45°S and 55°S are in near equilibrium with the atmosphere (Figure 1a). Cores PC75-2 (177°8.97′E, 44°14, 39′S; 967-m water depth) and PC83-1 (177°2,49′E, 44°18,38′S; 1,010-m water depth) were retrieved by the RV *Sonne* from the southern flank of the Chatham Rise east of New Zealand. The core locations are close to the modern position of the STF, which separates cold, less salty sub-Antarctic waters from warm, more saline subtropical waters (Coffin et al., 2013) and are bathed by Antarctic Intermediate Water (AAIW). Our core sites are located at the south edge of the subtropical CO_2 sink, with an annual mean modern ΔpCO_2= ~ −20 ppm and a modest seasonal cycle of ~30 ppm (Figure 1b and Figure S1 in the supporting information). Direct comparison between our paleo-reconstruction and modern ΔpCO_2 at the core site might be complicated by the following three factors (Figure S1): (1) Our site is potentially sensitive to front shifts during the last deglaciation: everything else being equal, a northward shift of the STF during the Last Glacial Maximum (LGM) and early deglaciation (Bostock et al., 2015) would turn our core site into a weaker sink or even a minor source; (2) a sediment trap study
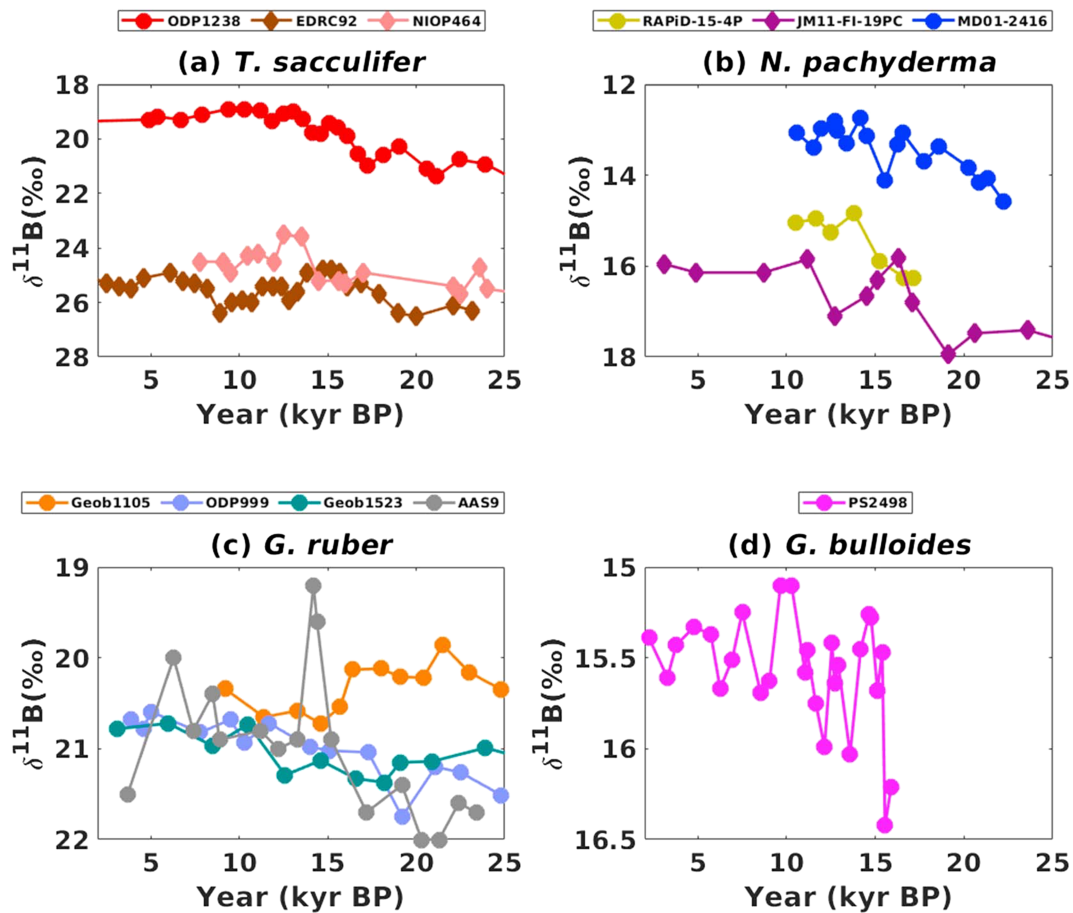
Figure 2. Twelve published boron records span the last deglaciation grouped into four species. (a) δ^{11}B measured in *Trilobatus sacculifer*, ODP1238 (red; Martínez-Botí et al., 2015), EDRC92 (brown; Palmer & Pearson, 2003) and NIOP464 (pink; Palmer et al., 2010). (b) δ^{11}B measured in *Neogloboquadrina pachyderma*, RAPiD-15-4p (yellow; Yu et al., 2013), MD01-2416 (blue; Gray, Weldeab, et al., 2018) and JM11-PI-19PC (dark purple; Ezat et al., 2017). (c) δ^{11}B measured in *Globigerinoides ruber*, GeoB1105 (orange; Foster & Sexton, 2014), ODP999 (light purple; Foster, 2008), GeoB1523 (dark green; Henehan et al., 2013) and AAS9 (gray; Naik et al., 2015). (d) δ^{11}B measured in *Globigerina bulloides* (magenta; Martínez-Botí et al., 2015). Records generated on a MC-ICPMS are marked with circles and records generated on a NTIMS are marked with diamonds. circles and records. MC-ICPMS = Multicollector-Inductively Coupled Plasma Mass Spectrometry; NTIMS = Negative Thermal Ionization Mass Spectrometry.

suggests that flux of *Globigerina bulloides* is much higher near our site between September to February, when the CO_2 sink is weaker than the rest of the year (Jonkers & Kučera, 2015); (3) strictly speaking, modern ΔpCO_2 may not be under a steady state (e.g., Holocene) due to anthropogenic CO_2 emissions.

2.2. Age Model for PC75-2 and PC83-1

2.2.1. Radiocarbon Measurements

For reconstruction of radiocarbon activities, mixed planktic and benthic foraminifera from PC75-1; *Globorotalia inflata (G. inflata)*, *G. bulloides*, and mixed benthic foraminifera from PC75-2; *G. inflata* from PC83-1 were picked (Table S1). For PC75-1, radiocarbon was measured at the Rafter Radiocarbon Lab at the GNS Science National Isotope Centre. For PC75-2 and PC83-1, ^{14}C dating was carried out at the Keck Carbon Cycle Accelerator Mass Spectrometry Laboratory at University of California, Irvine. Samples were leached in 10% dilute HCL immediately prior to hydrolysis.

2.2.2. Stable Isotope Measurements

Approximately 20–30 *G. inflata* were picked from PC75-2 and PC83-1 at each interval for δ^{18}O and δ^{13}C measurements. These were analyzed on a dual inlet VG Micromass Isoprime stable isotope ratio mass spectrometer equipped with an autocarbonate system at the University of Southern California. The precision of in-house calcite standards runs in conjunction with the foraminiferal samples averaged ~0.15‰ for δ^{18}O and ~0.06‰ for δ^{13}C (2 SD), over the course of the present study.

PC75-1 *G. inflata* and *Cibicides* $\delta^{18}O$ and $\delta^{13}C$ were analyzed by a Finnigan MAT 252 mass spectrometer at National Institute of Water and Atmospheric Research's stable isotope lab. Concurrently-run carbonate standards (NBS-19) had an internal precision of 0.08‰ for $\delta^{18}O$ and ~0.04‰ for $\delta^{13}C$ (2 SD).

2.2.3. Age Model

To develop an age model for the PC75 core location, we combined six new AMS ^{14}C dates measured on calcite tests of the planktic foraminiferal species *G. inflata* and *G. bulloides* from PC75-2 and four AMS ^{14}C dates from mixed planktic foraminifera from the colocated core PC75-1 core (Table S1). These two cores were taken from the same location but for different purposes. There was not enough material left from the PC75-1 core for both boron isotope analysis and radiometric dating. Therefore, samples from PC75-2 were used. The two cores have almost identical stratigraphies (Figure S2, Table S2). Each planktic ^{14}C age was converted to calendar years using the BChron Bayesian chronology package (Haslett & Parnell, 2008), with the marine calibration data set—MARINE13 (Reimer et al., 2013). This dating technique requires some knowledge of surface reservoir ages. Surface reservoir ages of the SW Pacific Ocean at various times during the last 25 kyr have been obtained in previous studies by pairing radiocarbon measurements of marine carbonates deposited above and/or below volcanic tephra layers (Sikes et al., 2000; Sikes & Guilderson, 2016; Skinner et al., 2015). The chronologic ages of the tephra have been constrained by radiocarbon dating terrestrial organic material from land-based deposits that contain the same tephra. By applying the up-to-date global calibration curve IntCal 13 (Reimer et al., 2013), Sikes and Guilderson (2016) concluded that surface reservoir ages during the late deglaciation and early Holocene were not significantly different from modern values. We therefore applied a reservoir age of 400 ± 100 yrs for each radiocarbon date from the core top to 110 cm, the oldest late deglacial interval where radiocarbon dates are available. We identified the "Kawakawa" tephra layer between 343 and 349 cm in core PC75-1. The tephra has a calendar age of 25,650 ± 40 years BP (Lowe et al., 2013; Sikes & Guilderson, 2016), which corresponds to an atmospheric ^{14}C age of 21,299 years according to the Intcal13 calibration. Right below this tephra layer, the planktic ^{14}C age at 350 cm is 22 904 years, which gives an estimate of late glacial reservoir age ~1,600 years. In a previous study using the same paired tephra-foraminifera dating technique on a core off New Zealand and locates just north of the subtropical/subpolar boundary, the estimated surface reservoir ages were ~1,000 years during the late glacial and ~1,250 years during the early deglaciation (Skinner et al., 2015). Taking these results together, we applied reservoir ages of ~1300 ± 200 years to our late glacial and early deglacial samples. To provide further age constraints, we utilized an additional chronologic datum: the beginning of the deglacial transition in the benthic $\delta^{18}O$ isotope stratigraphy of PC75-1, which occurs at 165 cm (Table S3). The regional deglacial transition at intermediate water depths of the SW Pacific has been dated at ~16,200–16,900 years BP (Stern & Lisiecki, 2014). We therefore, assigned an age of 16,500 ± 150 years BP to the 165-cm horizon. The calibrated ages from radiocarbon measurements and the two extra age control points (tephra layer and $\delta^{18}O$ transition) were used as tie points to develop the age model for PC75-2.

The age model for PC83-1 is based on 3 AMS ^{14}C dates, and the reservoir ages are same as those applied to the PC75 record since the two sites are very close to each other. An additional age constraint comes from aligning the stable isotope stratigraphy of PC75-2 and PC83-1 (Figure S3 and Table S2). For the intervals where there are no planktic ^{14}C dates or other age control, a linear interpolation has been used to estimate ages. We note that ages in PC83 are relatively uncertain, given the low resolution of our age control points, and this may be a source of uncertainty when comparing deglacial $\delta^{11}B$ data from these different sites. For a summary of applied reservoir ages and Bchron calibrated ages, see Table S4.

2.3. Trace Element and $\delta^{11}B$ Analyses

Approximately 100–200 tests of *G. bulloides* were picked from the 250- to 350-μm size fraction for trace element and $\delta^{11}B$ analyses (Table S5). Sample preparations were carried out in a low-boron clean lab at the University of St Andrews. Samples were cleaned based on the "Mg-cleaning" oxidation procedure (Barker et al., 2003; Rae et al., 2011). An aliquot (~3% of the total sample) was taken for trace element analyses, which were performed on an Agilent 7500 ICP-MS at the University of St Andrews using matrix-matched standards. Long-term reproducibility of Mg/Ca and B/Ca using this method is 1.2% and 2.3% (2 SD), respectively. Boron was separated from the sample matrix using Amberlite IRA-743 boron specific anion exchange resin, following the protocols of Foster (2008) and Foster et al. (2013). $\delta^{11}B$ was measured on a Thermo Scientific Neptune MC-ICP-MS at the University of St Andrews, based on protocols described in Foster (2008), Rae et al. (2011),

Rae (2018), but with the addition of high ohmage (10^{13} Ω) resistors and triplicate sample analyses. Samples were corrected for total procedural blank, which averaged 33 pg in this session. Rae et al. (2011) previously reported uncertainties of ±0.23‰ (2 SD) for samples of ~20 ng, increasing at smaller sample sizes. This has been improved given the developments in analyses described above. For example a boric acid standard (ERM-AE121; Vogl & Rosner, 2012) run during these sessions at the same concentration and under the same conditions as these samples (15 ppb) gave $\delta^{11}B = 19.59 \pm0.14$‰ (2 SD, $n = 8$); and replicate purifications and measurements of a dissolved carbonate standard with a composition mimicking planktic foraminifera, and run under these conditions at a concentration of 7 ppb, gave 2 SD of 0.20‰ ($n = 12$). However as full description and quantification of this updated method is beyond the scope of the current study, and as the signals found here are large compared to analytical uncertainty, we assign conservative analytical uncertainties following the relationships in Rae et al. (2011). Prior to $\delta^{11}B$ analysis, samples were screened for potential contamination by checking various elemental ratios (B/Ca, Mg/Ca, and Al/Ca). A few samples had elevated Al/Ca ratios (up to about 200–300 μmol/mol) but showed no correlation with either $\delta^{11}B$ or Mg/Ca (Figure S4).

2.4. Salinity Estimate:

To estimate sea surface salinity (SSS) changes, some authors have previously combined Mg/Ca and $\delta^{18}O$ of planktic foraminifera under the assumption that the amount of $\delta^{18}O$ change that cannot be accounted for by the Mg/Ca_x2010;derived temperature change must reflect a change in the oxygen isotopic composition of seawater, which is affected by salinity (Ezat et al., 2017; Naik et al., 2015). However, this approach assumes a constant relationship between salinity and the $\delta^{18}O$ of seawater; this assumption is unlikely to hold over G-IG time scales and can therefore result in large biases within the resulting salinity reconstruction. Given modeled regional changes in salinity are relatively small throughout most of the ocean during the LGM (Gray & Evans, 2019), we followed the approach outlined in Gray and Evans (2019) and calculate salinity as the modern salinity at our site plus the modeled mean surface ocean glacial salinity increase (0.7 PSU) scaled to global sea level (using the curve of Spratt & Lisiecki, 2016), with an uncertainty of ±1 PSU (2 SE). For any individual core, the two methods of salinity estimate would only introduce minor differences in reconstructed pH/pCO_2 values (Hönisch & Hemming, 2005). When developing a composite, one advantage of our approach is that removal of the long-term sea level influence on SSS, residual local SSS variations between sites are likely uncorrelated and would not systematically impact reconstruct pH/pCO_2 between sites.

2.5. Paired SST/pH and pCO$_2$ Estimate

The pH influences the Mg/Ca of planktic foraminifera (Evans et al., 2016; Gray, Weldeab, et al., 2018; Kısakürek et al., 2008; Lea et al., 1999; Russell et al., 2004). Temperature estimates from Mg/Ca are in turn required to calculate the boric acid and carbonate system dissociation constants (e.g., Dickson, 1990), and thus pH and pCO_2. Here, we apply a recently developed algorithm (Gray & Evans, 2019) that iteratively solves Mg/Ca and $\delta^{11}B_{borate}$ for SST and pH, overcoming the covariance induced between pH and temperature due to the thermal control on the carbonate system and boric acid disassociation constants. Mg/Ca_x2010;based SSTs estimated from this method are more consistent with alkenone-based SST estimates over deglaciation (Gray & Evans, 2019), thus carbonate system and boric acid dissociation constant estimates (and therefore pH and pCO_2) will also be more accurate. We use the *G. bulloides* Mg/Ca calibration given in Gray and Evans (2019), based on foraminifera grown in laboratory culture. Partial dissolution of planktic foraminiferal tests lowers Mg/Ca (Regenberg et al., 2014); we note, it does not affect $\delta^{11}B$ (Edgar et al., 2015). Here, we calculate temperature downcore as the temperature anomaly from the mean Holocene (0–10 ka) temperature, assuming the mean annual climatological temperature for the Holocene; this approach assumes that the effects of dissolution have remained approximately constant through time.

The ability to derive estimates of pH from the $\delta^{11}B$ of foraminiferal calcite stems from the fact that the borate ion is the dominant species incorporated into $CaCO_3$ (Hemming & Hanson, 1992; Rae, 2018; Rae et al., 2011). The methodology of transforming the boron isotopic composition of foraminifera to an estimate of ocean pH has recently been reviewed by Foster and Rae (2016) and Rae (2018). In the present study, $\delta^{11}B_{borate}$ is derived using the species-specific calibration for *G. bulloides* determined by a Monte Carlo/wild bootstrap approach (Henehan et al., 2016), where $\delta^{11}B_{borate} = (\delta^{11}B_{CaCO3} + 3.58 \pm 11.77)/1.09 \pm 0.65$ (Raitzsch

et al., 2018), which has a wider range of uncertainty than used by Martínez-Botí et al. (2015). The $\delta^{11}B_{borate}$ value is then used to estimate pH using the accurate formula from Rae (2018).

The estimate of local seawater pCO_2 from the pH value requires an assumption about a second parameter of the carbonate system, typically the local sea surface alkalinity (ALK), which is poorly constrained for the glacial and deglacial ocean. To estimate sea surface ALK some authors have applied a modern local SSS-ALK regression relationship, using estimates of paleo-SSS (Ezat et al., 2017; Martínez-Botí et al., 2015; Naik et al., 2015). This assumes that most of the variability in ALK and SSS are dominated by evaporation and precipitation and/or sea level changes. However, SSS and ALK could be decoupled due to changes in riverine input of ALK, nutrient uptake, remineralization, and production and export of $CaCO_3$ (Fry et al., 2015). Thus, applying the modern local SSS-ALK regression could introduce significant bias. In a previous study, Martínez-Botí et al. (2015) randomly varied ALK between the modern value at the site today +125 μmol/kg (Hain et al., 2010; Toggweiler, 1999) to −25 μmol/kg with a flat distribution given that knowledge of the secular evolution of ALK during the last deglaciation is currently lacking. However, it is possible that, even with higher whole ocean alkalinity, sea surface ALK was not much different from modern values due to stronger ocean stratification and the deep remineralization profile of $CaCO_3$. We therefore randomly vary ALK between "modern +75 μmol/kg" to "modern −75 μmol/kg" in each pCO_2 calculation. Note that this uncertainty range is large, encompassing much of the variability of the modern ocean. Also, resulting uncertainty on pCO_2 remains dominated by the uncertainty on $\delta^{11}B$-derived pH, given the close coupling of pH and CO_2 within the carbonate system (Rae, 2018).

The pH and seawater pCO_2 for each sample horizon is calculated using the "seacarb" package in R (https://CRAN.R-project.org/package=seacarb). To fully propagate the uncertainties associated with pH/pCO_2 estimations, we ran 10,000 Monte Carlo simulations that included the following uncertainties (2 SE): analytical uncertainty on $\delta^{11}B_{CaCO3}$, salinity ± 1 PSU, Mg/Ca calibration uncertainty, $\delta^{11}B_{CaCO3} - \delta^{11}B_{borate}$ calibration uncertainty.

2.6. Composite pH and Seawater pCO_2

We compiled 10 previously published and two new (this study) boron-based pH/seawater pCO_2 reconstructions with millennial-scale resolution spanning the last 25 kyr. RAPiD-15-4P (Yu et al., 2013) is not included in the composite because both Holocene and LGM intervals are missing in this record (Figure 2). We recalculated pH and seawater pCO_2 from each published boron isotope value with a self-consistent framework. This includes modifying published estimations of (1) SST; (2) SSS; and (3) the carbonate $\delta^{11}B$ to $\delta^{11}B_{borate}$ in seawater. The SSS and SST changes for each record are recalculated in the manner described in sections 2.4 and 2.5, with species-specific Mg/Ca calibrations from Gray and Evans (2019). Calculating seawater $\delta^{11}B_{borate}$ from the foraminiferal $\delta^{11}B$ under a self-consistent framework is not a trivial task since the records were generated using different machines and/or techniques. The pioneering work on the species-specific $\delta^{11}B$ calibration was conducted on Negative Thermal Ionization Mass Spectrometry (NTIMS; Sanyal et al., 1996, 2001). More recently, Multicollector-Inductively Coupled Plasma Mass Spectrometry (MC-ICPMS) has been used for boron isotope analyses of marine carbonates (Foster, 2008). However, measured $\delta^{11}B$ from the same planktic species (see, e.g., Figure 2a) or even homogenized calcite samples (Farmer et al., 2016) are lower on ICPMS than NTIMS by up to several per mil in some cases. Currently, this technique offset is not easily explained (see Farmer et al., 2016) but may be possible to correct. Logically, the same slopes "m" (i.e., pH sensitivities) should be applied to all records using the same species, no matter which technique was used to generate the boron isotope data. Indeed, studies suggest that the calibration slope may be transferable between different measurement techniques (Farmer et al., 2016; Foster et al., 2013). Therefore, the correction involves applying a constant offset to the established species-specific calibrations.

The slope ("m") of the foraminiferal $\delta^{11}B_{CaCO3}$ versus $\delta^{11}B_{borate}$ in seawater has been determined through culturing, core top and sediment trap data sampling using both techniques (Henehan et al., 2013; Martínez-Botí et al., 2015; Sanyal et al., 2001). Our strategy is to apply the latest species-specific calibration curves that include newer data and more robust statistical techniques. The calibration curve for *Globigerinoides ruber* and *G. bulloides* comes from Raitzsch et al. (2018). For *Trilobatus sacculifer*, the intercept presented in Raitzsch et al. (2018) is offset from that of Henehan et al. (2016) by ~0.8‰ with essentially the same slope. This is because one culture data point from Sanyal et al. (2001) was misplaced (i.e., one

$\delta^{11}B_{CaCO_3}$ data should be 18.49‰ not 18.9‰) by Raitzsch et al. (2018) and more core top data were included in that study. To let our recalculated pH/pCO$_2$ be close to original published values, we chose the calibration curve from Henehan et al., 2016 for *T. sacculifer*. The calibration used for *Neogloboquadrina pachyderma* (*N. pachyderma*) is $\delta^{11}B_{borate} = \delta^{11}B_{CaCO_3} +3.38 \pm 0.72$‰ (first calibrated by Yu et al., 2013, later confirmed by Gray, Weldeab, et al., 2018 over a wider range of pH). For the *N. pachyderma* JM11 record generated by NTIMS (Ezat et al., 2017), we used the original intercept of 2.053‰ (Ezat et al., 2017, NTIMS) instead of 3.38‰ (Gray, Weldeab, et al., 2018, MC-ICP-MS) to account for technique/machine offsets. Applying the *T. sacculifer* calibration curve to the Holocene $\delta^{11}B$ of NIOP464 (Palmer et al., 2010, NTIMS) and EDRC92 (Palmer & Pearson, 2003, NTIMS) resulted in very different pH from the original publication, due to technique/machine offsets. Thus, we modified the intercept such that the average Holocene pH from each record equals the preindustrial sea surface pH at the core site that is derived from the GLODAP V2 2016b data set. Table 1 summarizes the regression applied for each individual record. Where possible we use reported analytical uncertainty of $\delta^{11}B$; Palmer and Pearson (2003) and Palmer et al. (2010) did not report analytical uncertainties, so we use ± 0.3‰ (2 SE). The procedure described in section 2.5 is then applied to calculate pH and pCO$_2$ for each data point. We term the results as pH$_{boron}$ and pCO$_{2boron}$. When we developed the pH and pCO$_2$ composite, we treated each pH$_{boron}$ and pCO$_{2boron}$ data point as a sample of the global mean sea surface pH and pCO$_2$. However, $\delta^{11}B$-based pH reconstructions may carry a bias relative to the true mean pH at a specific sample site ("reconstruction bias") and true mean pH at each site carries a bias relative to mean global pH ("location bias"). For each individual record, the reconstruction bias is estimated by the difference between the average pH$_{boron}$ over the Holocene (pH$_{boron\_Holocene}$) and preindustrial pH at that site (pH$_{site\_preind}$) from the GLODAP V2 2016b product (Lauvset et al., 2016); the location bias is estimated by the difference between pH$_{site\_preind}$ and the global preindustrial pH from the same GLODAP product ("pH$_{global\_preind}$"). The expression for the final pH data is then: pH$_{final}$ = pH$_{boron}$ − (pH$_{boron\_Holocene}$ − pH$_{site\_preind}$) − (pH$_{site\_preind}$ − pH$_{global\_preind}$) = pH$_{boron}$ − pH$_{boron\_Holocene}$ + pH$_{global\_preind}$. The uncertainty of "pH$_{boron\_Holocene}$" and "pH$_{global\_preind}$" are then propagated into using 10,000 Monte Carlo simulations, along with a ± 700-year age error (2 SE) for each sample age. The same procedure is applied to pCO$_2$: pCO$_{2final}$ = pCO$_{2boron}$ − (pCO$_{2boron\_Holocene}$ − pCO$_{2site\_preind}$) − (pCO$_{2site\_preind}$ − pCO$_{2global\_preind}$) = pCO$_{2boron}$ − pCO$_{2boron\_Holocene}$ + pCO$_{2global\_preind}$. The final pH/pCO$_2$ data from each of the cores were then binned into 1,000-year intervals, and the average pH/pCO$_2$ for each bin was calculated.

We note here that when we discuss the deglacial history of sea surface pH/pCO$_2$ in the SW Pacific in sections 3.1 and 4.1, we report and refer to the uncorrected pH$_{boron}$ and pCO$_{2boron}$ values from PC75-2 and PC83-1. On the other hand, when we discuss the global composite pH/pCO$_2$ in sections 3.2 and 4.2, we refer to the corrected pH$_{final}$ and pCO$_{2final}$ from 12 records.

2.7. Modeling the GMSSpH With cGENIE Earth System Model

The Earth System model cGENIE was used to develop a simulated GMSSpH over the last 25 kyr to compare against the composite pH curve. The cGENIE model includes a 3-D dynamical ocean model coupled to the 2-D energy-moisture balance atmospheric model (Edwards & Marsh, 2005). The ocean model is based on a 36 × 36 horizontal grid with 16 vertical layers. cGENIE has a dynamic and thermodynamic component of sea ice. The model also incorporates a marine biogeochemical cycling of carbon and other tracers (Ridgwell et al., 2007). All simulations in the present study used a preindustrial configuration (Cao et al., 2009) and were spun up as a closed system for 20 kyr.

To estimate the GMSSpH over the last 25 kyr, an LGM-like sea surface carbonate chemistry state is a necessary initial condition for the model. Since an investigation of carbonate system feedbacks is not the purpose of this study, interactive sediments (i.e., open-system configurations) are not used in the following simulation. We achieved a peak glacial atmospheric pCO$_2$ value through an inverse approach with three end-member scenarios. Specifically, in scenario 1 ALK is added to the surface ocean; in scenario 2 ALK and DIC are added to the surface ocean in a 2:1 ratio (i.e., CaCO$_3$ addition); in scenario 3 DIC is subtracted from the surface ocean. We performed the inversion under a modern ocean circulation for 10,000 years. The resulting LGM atmospheric pCO$_2$ and seawater chemistry responses at the end of the inversion are summarized in Table 2. Since the GMSSpH is strongly coupled to the atmospheric pCO$_2$, we would get essentially the same answer even if we apply an LGM-like circulation scenario (not shown). Then, to estimate the GMSSpH over

Table 1

Calibration Curves Used for Each Individual Record; Regression in the FOrm of $\delta^{11}B_{CaCO3} = m* \delta^{11}B_{borate} +c$

Core name	Species	Slope ("m")	Intercept ("c")	Reference	Calibration	Technique
ODP1238	*Trilobatus sacculifer*	0.82	3.94	Martínez-Botí et al. (2015)	Henehan et al. (2016)	MC-ICP-MS
NIOP464	*T. sacculifer*	0.82	−0.66	Palmer et al. (2010)	Henehan et al. (2016) "c" modified by this study	NTIMS
EDRC92	*T. sacculifer*	0.82	−1.66	Palmer and Pearson (2003)	Henehan et al. (2016) "c" modified by this study	NTIMS
MD01-2416	*Neogloboquadrina pachyderma*	1	−3.38	Gray, Weldeab, et al. (2018)	Gray, Weldeab, et al. (2018)	MC-ICP-MS
JM11-PI-19PC	*N. pachyderma*	1	−2.053	Ezat et al. (2017)	Gray, Weldeab, et al. (2018), "c" modified by Ezat et al. (2017)	NTIMS
ODP999	*Globigerinoides ruber*	0.55	9.82	Foster (2008)	Raitzsch et al. (2018)	MC-ICP-MS
GeoB1523	*G. ruber*	0.55	9.82	Henehan et al. (2013)	Raitzsch et al. (2018)	MC-ICP-MS
GeoB1105	*G. ruber*	0.55	9.82	Foster and Sexton (2014)	Raitzsch et al. (2018)	MC-ICP-MS
AAS9	*G. ruber*	0.55	9.82	Naik et al. (2015)	Raitzsch et al. (2018)	MC-ICP-MS
PS2498-1	*Globigerina bulloides*	1.09	−3.58	Martínez-Botí et al. (2015)	Raitzsch et al. (2018)	MC-ICP-MS
PC75-2	*G. bulloides*	1.09	−3.58	this study	Raitzsch et al. (2018)	MC-ICP-MS
PC83-1	*G. bulloides*	1.09	−3.58	this study	Raitzsch et al. (2018)	MC-ICP-MS

the last 25 kyr, a transient carbon flux was added or taken out of the atmosphere so that the atmospheric pCO_2 follows the ice core record.

3. Results

3.1. Two New Boron Isotope-Based pH Reconstructions From the SW Pacific

The new $\delta^{11}B$ record from subtropical South Pacific core PC75-2 is shown in Figure 3a. This core documents ~1.5‰ lower values during the early deglacial relative to the glacial and late deglacial samples and shows a pronounced excursion to low $\delta^{11}B$ values around 16.5–14 kyr BP. The record from core PC83-1 spans the last 16 kyr (Figure 3e). In this core, the $\delta^{11}B$ values in both the early deglacial section and the Holocene section are close to 15–15.5‰, while values from the late deglacial section and the core top are characterized by values of ~16‰. Once converted to pH (Figures 3c and 3g) these records demonstrate the surface/shallow subsurface pH in the SW Pacific was ~8.2 during the LGM and early deglaciation, before being punctuated by low pH values between ~16.5 and 14 kyrBP (Figure 3c). The pH values are around ~8.1 in the late deglaciation and early Holocene and rise to 8.2 at the core top (~2.3 kyr BP). The pCO_2 reconstruction at our site suggests on Chatham Rise, sea surface pCO_2 were up to ~300 to 450 μatm during the last deglaciation and early Holocene.

Table 2

Scenarios to Achieve Atmospheric pCO_2 ~ 180 ppm Through Surface Inversion in cGENIE

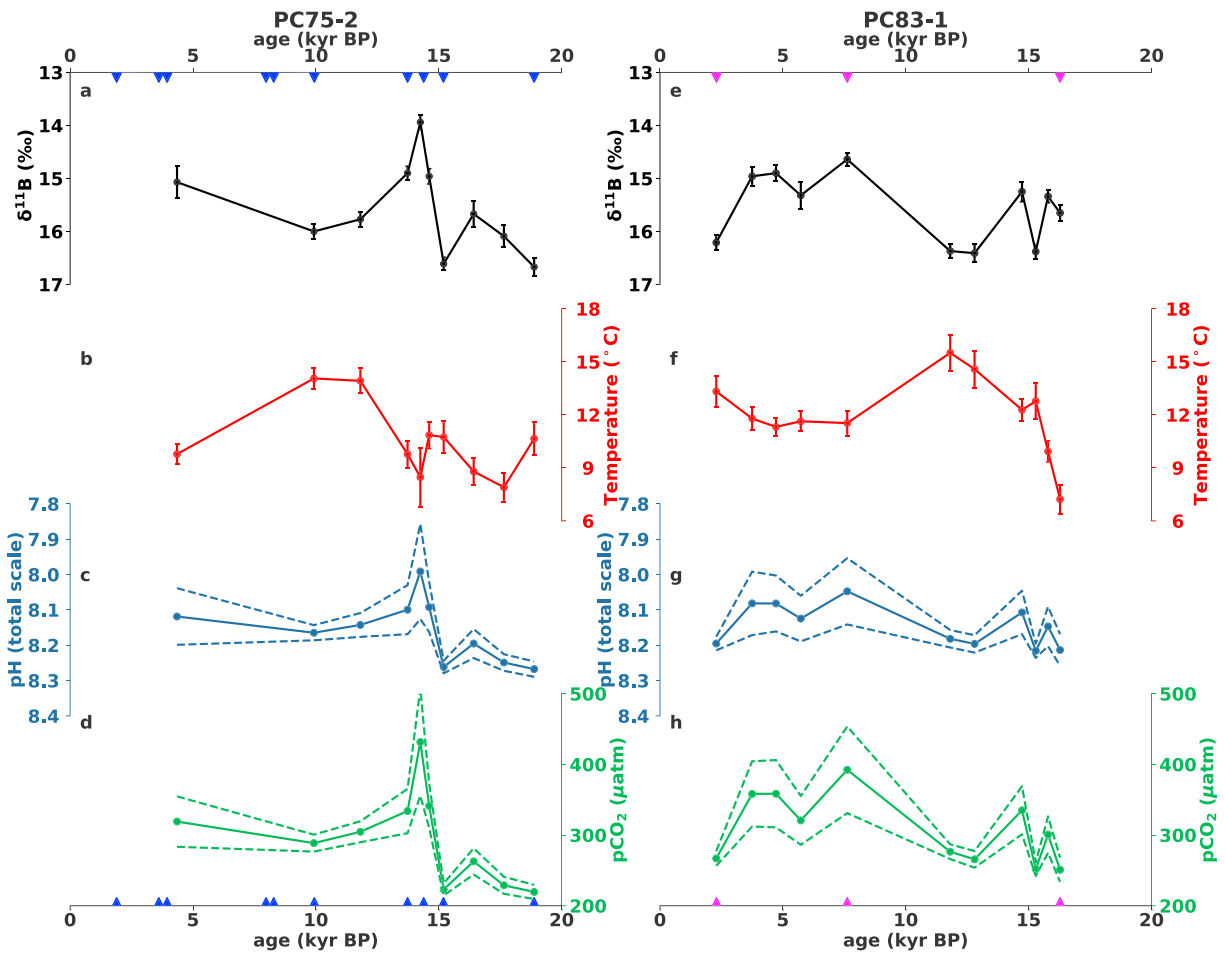| Experiment name	Spin	ALK addition	CaCO₃ addition	DIC removal
Atm pCO_2 (ppm)	278	184	184	181
Surface pH (total scale)	8.15	8.31	8.34	8.30
Surface ALK (μmol/kg)	2,268	2,350	2,542	2,264
Surface DIC (μmol/kg)	1,953	1,937	2,084	1,871

Figure 3. Deglacial changes in seawater carbonate chemistry and sea surface temperature (SST) of Chatham Rise. (a–d), PC75-2; (e–h), PC83-1. (a, e) *G. bulloides* $\delta^{11}B$ (versus boric acid standard NIST 951) with analytical uncertainties (2 SE). (b, f) *G. bulloides* Mg/Ca-based SST with uncertainties (1 SE). (c, g) $\delta^{11}B$-based pH. (d, h) $\delta^{11}B$-derived pCO_2. The dotted envelopes represent uncertainty of sea surface pH and pCO_2 (1 SE). Triangle marks represent intervals with radiocarbon age constraints.

Table 3

Estimated pH_{boron_Holocene}, pH_{site_preind}, pCO_{2boron_Holocene} and pCO_{2site_preind} for 12 individual records with errors (1SE)

Core name	$pH_{boron\_Holocene}$ (total scale)	pH_{site_preind} (total scale)	$pCO_{2boron\_Holocene}$ (μatm)	pCO_{2site_preind} (μatm)
PC83	8.106 ± 0.023	8.214 ± 0.119	339 ± 19	265 ± 77
PC75	8.142 ± 0.016	8.214 ± 0.119	304 ± 11	265 ± 77
NIOP464	8.095 ± 0.015	8.091 ± 0.020	351 ± 15	355 ± 19
ODP1238	8.107 ± 0.010	8.081 ± 0.027	335 ± 9	353 ± 26
ODP999	8.161 ± 0.007	8.138 ± 0.055	286 ± 5	312 ± 46
GEOB1105	8.123 ± 0	8.159 ± 0.019	324 ± 0	294 ± 15
GEOB1523	8.175 ± 0.006	8.155 ± 0.002	276 ± 5	290 ± 2
AAS9	8.245 ± 0.013	8.192 ± 0.054	228 ± 9	262 ± 39
EDRC92	8.099 ± 0.011	8.091 ± 0.033	332 ± 10	337 ± 29
JM11	8.249 ± 0.007	8.240 ± 0.002	233 ± 5	236 ± 1
MD01-2416	8.158 ± 0	8.200 ± 0.005	289 ± 0	258 ± 4
PS2498	8.154 ± 0.007	8.193 ± 0.013	298 ± 5	267 ± 9

Note. The uncertainty for MD01-2416 and GeoB1105 record is 0 because there is only one data point in the entire Holocene period. Global mean preindustrial sea surface pH = 8.18, sea surface pCO_2 = 271 ppm. The terms pH_{site_preind} and pCO_{2site_preind} are not part of the expression to calculate pH_{final} and pCO_{2final} (see the main text) as they are canceled out when both the reconstruction bias and the location bias are taken into account.
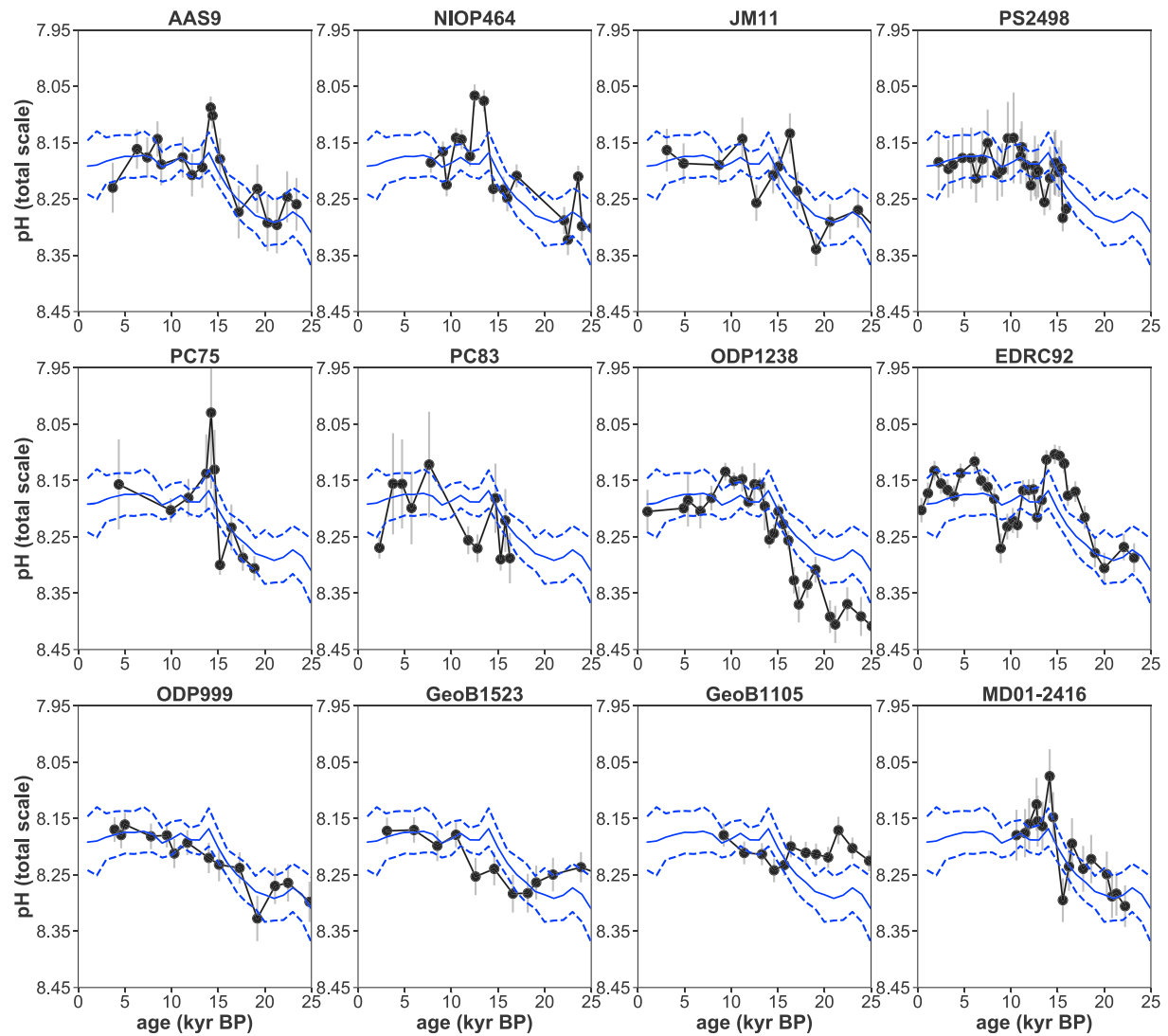
Figure 4. Individual pH reconstructions (corrected for "location bias," that is, $pH_{final} = pH_{boron} - pH_{boron\_Holocene} + pH_{global\_preind}$) plotted against the composite pH.

3.2. The pH and Seawater pCO₂ Composite Versus the Simulated GMSSpH

Table 3 summarizes the estimated $pH_{boron\_Holocene}$, pH_{site_preind}, $pCO_{2boron\_Holocene}$, and pCO_{2site_preind} for 12 individual records. Based on these estimations, the location bias and the reconstruction bias are corrected. Individual pH records are shown against the composite pH in Figure 4. The pH and pCO₂ composite are built on 219 boron isotope data from 12 cores sites (Figure 5a and 5b). The pH values from ODP999 closely follows the median composite, while in most other cases, an individual record generally fluctuates around the median composite, with a few data points falling outside of the 95% envelop of the composite (Figure 4). Some recognizable patterns are as follows: (1) During the LGM and early deglaciation (25–15 kyr BP), the ODP1238 record consistently shows higher pH, while the GeoB1105 record shows lower pH than the composite; (2) AAS9, NIOP464, PC75-2, EDRC92, and MD01-2416 all show anomalously low pH values between 15 and 14 kyr BP; (3) During the late deglaciation (15–10 kyr BP), although some data points from GeoB1523, GeoB1105, and PC83-1 are close to the composite, other pH values are higher than the composite mean. We emphasize here again that the above description is based on corrected pH values (i.e., pH_{final}) in this study, which should not be confused with conclusions drawn from uncorrected pH values (e.g., section 3.1 for our
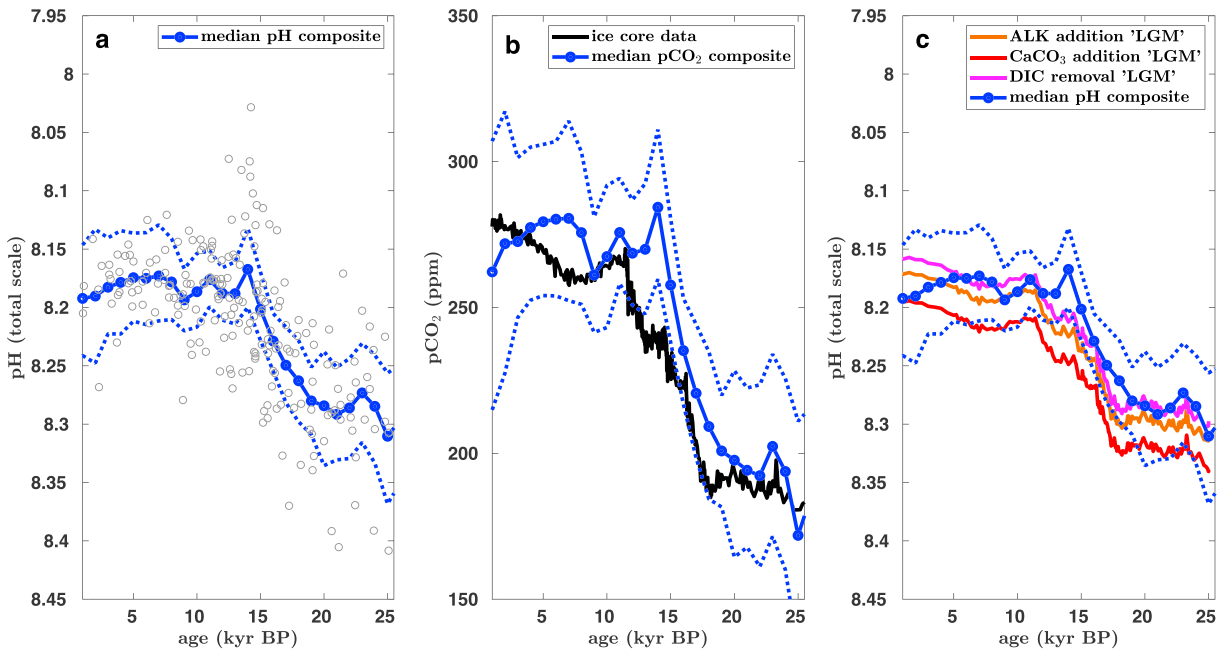
Figure 5. Composite pH and pCO$_2$. (a) The blue solid line denotes the median of the 10,000 simulations of the composite pH values. The blue dotted line denotes the 95% quantiles of the 10,000 simulations of the composite pH values. The gray dots represent individual boron isotope-derived pH ($n = 219$) after corrections (i.e., pH$_{final}$). (b) Composite seawater pCO$_2$ versus the ice core record of atmospheric CO$_2$. The solid blue line denotes the median of the 10,000 composite pCO$_2$. The blue dotted line denotes the 95% quantile of the 10,000 composite pCO$_2$. The solid black line represents the ice core record of atmospheric pCO$_2$. (c) Composite pH versus cGENIE inverted pH. The blue lines are the same as in panel (a). The brown, red, and magenta solid lines denote the cGENIE-simulated GMSSpH evolution where the initial conditions are achieved through "ALK addition," "CaCO$_3$ addition" and "DIC removal," respectively.

data and original publications for other records.). For reference, individual uncorrected pH records (i.e., pH$_{boron}$) are plotted with the composite in Figure S5.

The composites are developed from 12 cores that come from a wide range of oceanographic settings. At sites where the carbonate system is strongly affected by seasonality and the fluxes of planktic foraminiferal tests have distinct seasonal patterns, the pH and thus pCO$_2$ estimates will likely be biased toward the season of maximum production. Also, since foraminifers calcify over a range of depths instead of strictly at the surface, the composite may be biased toward higher pCO$_2$ because seawater pCO$_2$ increases with depth within the top few hundreds of meters (Ezat et al., 2017; Raitzsch et al., 2018; Taylor et al., 2018; Yu et al., 2013). However, we found that these complexities would only have minor effects on our composite pCO$_2$ (Figures S6 and S7), probably because the calibrations that are largely based on core top measurements that already account for some of these effects.

Three scenarios of simulated GMSSpH over the last 25 kyr are presented in Figure 5c; these curves follow the same deglacial structure, due to the close coupling between pCO$_2$ and surface ocean pH, but have different absolute values, due to their different alkalinity and DIC (Table 2). For a given pCO$_2$, DIC removal results in slightly lower pH than alkalinity addition, while addition of alkalinity and DIC in a 2:1 ratio (CaCO$_3$ addition) gives higher pH with a larger offset, due to the larger change in ALK-DIC chemistry in this scenario. Our three scenarios provide different end member GMSSpH solutions for glacial pCO$_2$, and the real sea surface carbonate chemistry condition at the LGM and thus the real deglacial GMSSpH evolution likely falls in the range of the three curves in Figure 5c. The δ^{11}B-derived pH and pCO$_2$ composites match the overall trend of the GMSSpH simulated by cGENIE and the atmospheric record of pCO$_2$, respectively (Figures 5b and 5c, and Table S6). However, during the last deglaciation, the composite pH is generally lower than all three simulated GMSSpH, and correspondingly, the composite pCO$_2$ is generally higher than the contemporary atmosphere. pCO$_2$ disequilibrium in the deglaciation is quite robust, given that this interval has the best data coverage, and the lower 2.5% quantile also falls above the atmospheric pCO$_2$ record (Figure 5b).
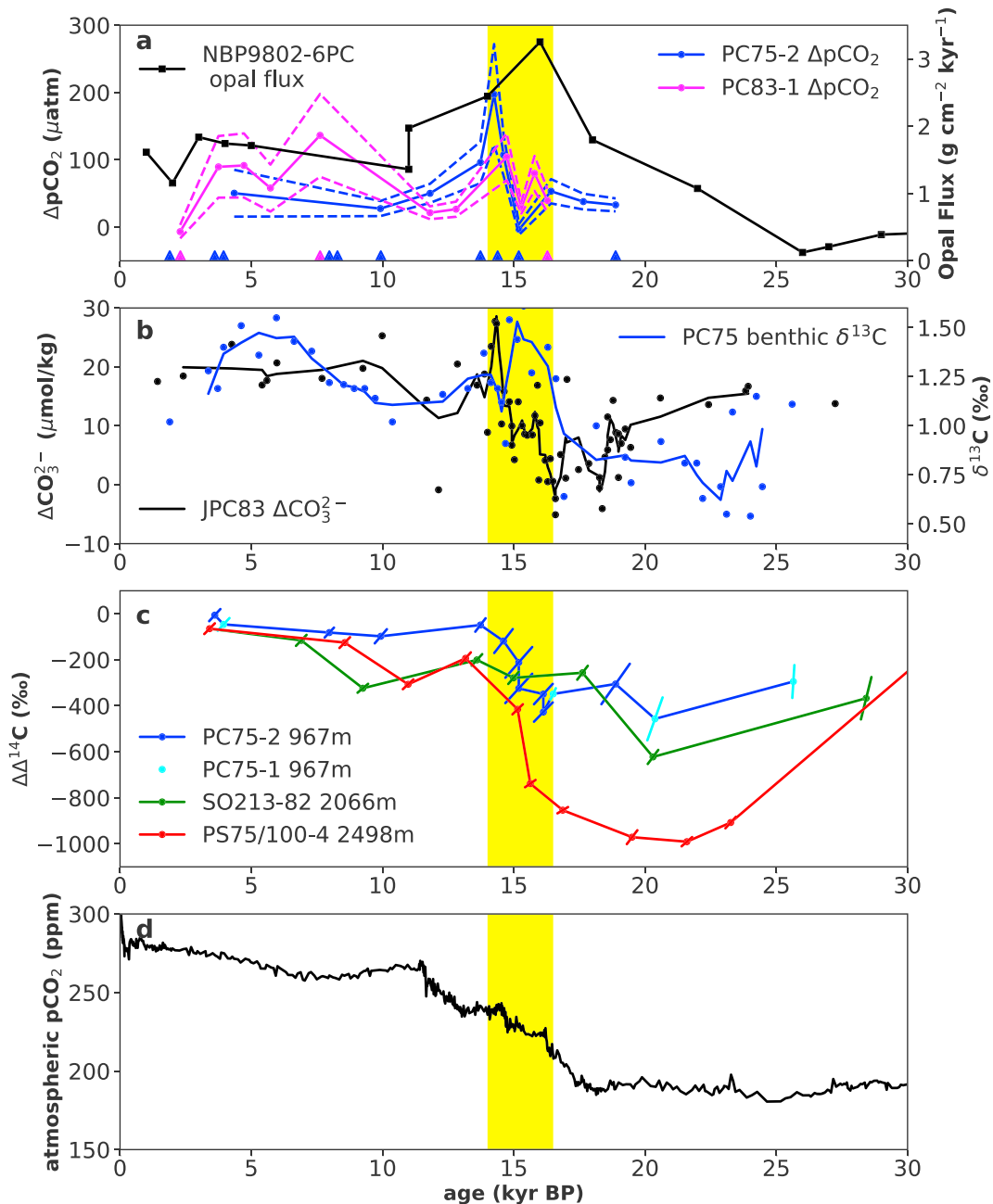
Figure 6. (a) PC75-2 and PC83-1 ΔpCO_2 plotted with an opal flux record from the SW Pacific sector of the Southern Ocean (Chase et al., 2003). The dotted envelopes represent uncertainty of ΔpCO_2 (the 14% and 86% quantile). Triangle marks represent intervals with radiocarbon age constraints as in Figure 3. (b) JPC83 benthic $\Delta[CO_3]^{2-}$ from the Bay of Plenty (Allen et al., 2015), plotted with PC75-1 (this study) benthic $\delta^{13}C$ records. The raw data are plotted as dots; the thick lines are three-point running averages. (c) Three records of benthic-atmospheric $\Delta^{14}C$ offset ($\Delta\Delta^{14}C$) from Chatham Rise. PC75-1 and PC75-2 radiocarbon data are combined together but are labeled with different color coding. (d) Atmospheric pCO_2 (Bereiter et al., 2015). The 16.5–14 kyr BP event is highlighted in yellow for all panels.

4. Discussion

4.1. Chatham Rise as a Source of Carbon to the Atmosphere Over the Last 19 kyr.

Results presented in this study indicate that the subtropical-subpolar transition zone of the SW Pacific was a site of carbon ventilation during the last deglaciation (Figure 6a), whereas in the modern ocean this region is a modest carbon sink (Figures 1a and S1). A similar result was observed at a South Atlantic site (Martínez-Botí et al., 2015) that is also a sink region in the modern ocean. Together, these results suggest that both the

Atlantic and Pacific sectors of the Southern Ocean became sources of CO_2 to the atmosphere during the deglaciation.

We acknowledge that our cores are of low resolution, therefore the two records may not resolve the complete history of surface ΔpCO_2 in this region. We note that for many time intervals we do not have overlapping data from both cores, thus it is not possible to rule out that the offsets seen between the two cores may represent higher-frequency variability than is captured by the resolution of each core. There are also mismatches in reconstructed pH/_x0394;pCO_2 at apparently overlapping time intervals between the two records, but due to age model uncertainties (note there are only three radiocarbon dates to constrain the age model of PC83-1, see the magenta triangle markers in Figures 3 and 6) and low resolution, it is possible that these intervals of apparent mismatch do not truly represent overlapping time intervals, as evidenced by some notable differences in Mg/Ca_x2010;based SST between these records. With the above caveats in mind, we now discuss the main signals in the boron isotope data in context with other paleoceanographic proxies in this region.

4.1.1. Possible Geological Carbon Influence on Our Site on Chatham Rise

Two cores from Chatham Rise document extreme negative benthic $\Delta^{14}C$ values between 2,000 and 3,000 m at the last glacial termination (Ronge et al., 2016). Ronge et al. (2016) hypothesized that these sites record the influence of radiocarbon-dead hydrothermal CO_2 transported from the East Pacific Rise. However, it is unlikely that such large $\Delta^{14}C$ anomalies from volcanic degassing of CO_2 from the East Pacific Rise would reach Chatham Rise without losing their highly ^{14}C-depleted radiocarbon signature (Ronge et al., 2016). Also, there are no known hydrothermal systems near Chatham Rise that could provide such ^{14}C-depleted carbon.

Large pockmarks have been identified across the southern edge of the Chatham Rise in seismic sections (Davy et al., 2010), close to the cores that document large negative $\Delta\Delta^{14}C$ anomalies (this study and Ronge et al., 2015). Davy et al. (2010) previously hypothesized that the pockmarks formed at glacial terminations during the Pleistocene and argued that they came about in response to destabilization of methane hydrates. A subsequent research cruise was conducted in 2013 to explore for methane hydrates, but none of the data from that investigation support there being a flux of methane through the sediment (Coffin et al., 2013), which suggests the pockmarks formed in response to release of old geologic CO_2 rather than CH_4 (Stott et al., in revision). It appears from seismic profiles that pockmarks have recurred through the Pleistocene and therefore there have been recurrent episodes of geologic carbon release through these pockmarks on the Chatham Rise during earlier glacial cycles. Our PC75 core was taken in close proximity to one of the large pockmarks as was the core studied by Ronge et al. (2016).

Today, our PC75 core site is bathed by well-ventilated, relatively "young" AAIW. However, between 25 and 16 kyr BP, the benthic radiocarbon values were much more depleted compared to the contemporaneous atmosphere ($\Delta\Delta^{14}C$ of ~300–400‰; Figure 6c). This atmosphere-benthic $\Delta^{14}C$ offset is much larger than values from corals collected at slightly deeper water depths in the Tasman Sea (Hines et al., 2015; regardless of our assumptions about surface reservoir ages, see Figure S8). These data, together with the results of Ronge et al. (2016), indicate that there were local sources of much older carbon at the Chatham Rise between 25 and 16 kyr BP.

Our boron isotope data only extends to 20 kyr. Over this period ΔpCO_2 values range between 0 and 80ppm in the PC75-2 record. It is possible that some of the old carbon that was responsible for the benthic $\Delta^{14}C$ excursions reached surface waters, which could account for the elevated surface ocean pCO_2 and the anomalously old surface reservoir ages (Sikes & Guilderson, 2016; Skinner et al., 2015; see a conceptual diagram for the LGM, Figure 7b). This idea will require additional evaluation but the fact that the pockmarks, the $\Delta^{14}C$ anomalies, including those documented by Ronge et al. (2016), and elevated pCO_2 values coincided suggest that they may have been mechanistically linked. And the fact that the atmosphere-benthic $\Delta\Delta^{14}C$ values remained low for several thousand years further suggests there was a substantial and relatively continuous supply of old carbon and perhaps reduced ventilation between 900 and 2,500 m of the SW Pacific that prolonged the $\Delta\Delta^{14}C$ anomaly during the early deglaciation.

4.1.2. Surface Ocean pCO_2, 16.5–14 kyr

The interval from 16.5–14 kyrBP is characterized by the most prominent CO_2 outgassing event in our reconstruction (Figure 6a, shaded in yellow). There are five data points from the two records that suggest the surface ΔpCO_2 was up to +100 ppm during this period. Notably, the peak outgassing coincided with periods of rapidly rising atmospheric CO_2 (~16.3 and 14.8 kyr BP; Marcott et al., 2014; Figure 6d). This outgassing event
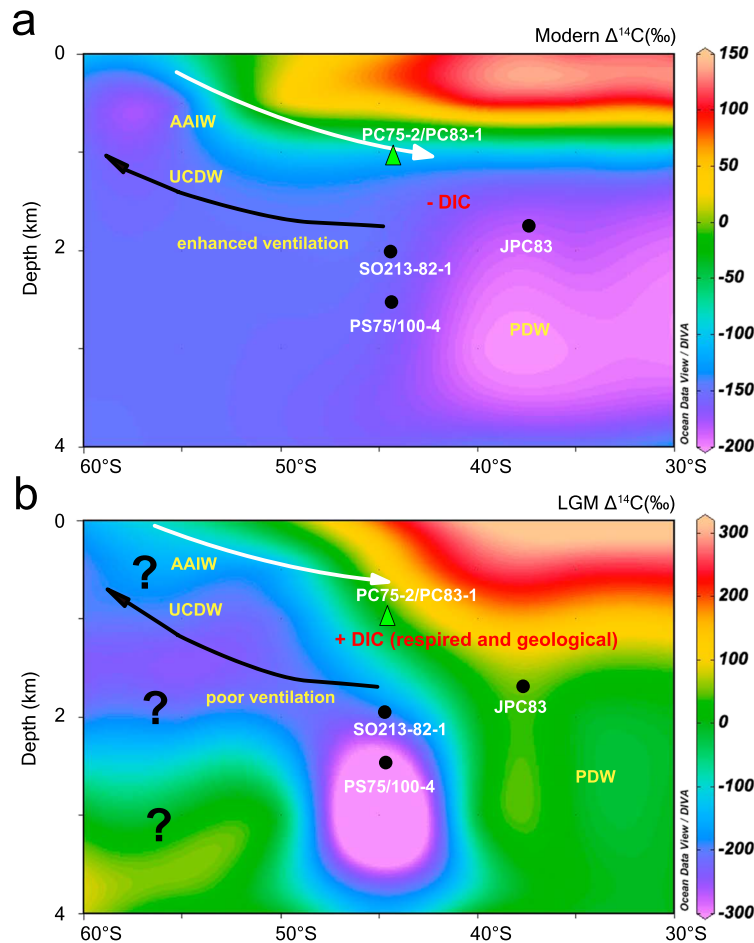
Figure 7. Conceptual diagrams of SW Pacific circulation and radiocarbon distribution. (a) Modern pattern. Sites PC75-2 and PC83-1 are bathed under well-ventilated AAIW, with no influence of geological carbon. The color shading is based on interpolating a transect of Δ^{14}C data between 170°E to 180°E from the GLODAP database to a 10° in latitude by 500 m in depth grid. (b) LGM pattern. Site PC75-2 and site PC83-1 are bathed under poorly ventilated, respired carbon-rich UCDW. Episodic release of ^{14}C-dead geological carbon makes the deep/intermediate waters as well as the surface of Southern Ocean appear to be "old." The color shading is based on multiple published Δ^{14}C records from sediment cores (not labeled in the panels) that represent glacial Δ^{14}C signature of PDW, AAIW, and SAMW in the Southern Hemisphere. The high-latitude Southern Ocean is labeled with question marks due to a lack of data. Panels were generated using ODV 4.7.10. AAIW = Antarctic Intermediate Water; LGM = Last Glacial Maximum; UCDW = Upper Circumpolar Deep Water; PDW = Pacific Deep Water; SAMW = Sub-Antarctic Mode Water.

at the surface is also closely associated with a rapid rise in carbonate ion saturation at middepths of the Southwest Pacific (Allen et al., 2015; Figure 6b) and thus, an apparent loss of carbon from middepth deep waters (assuming that alkalinity is unlikely to change this dramatically). At the same time, benthic $\Delta\Delta^{14}$C (this study; Ronge et al., 2016) returned to younger (Figure 6c, see Table S7 for the Δ^{14}C data), Holocene-like values, suggesting enhanced ventilation of the intermediate depths of the Southwest Pacific.

Between 16.5 and 14 kyr BP, there was a rapid 0.5‰ increase in benthic δ^{13}C values, followed by a 0.3‰ decline at our site. This pattern is also observed in the MD97-2120 and 79JPC records from the SW Pacific and the MD07-3088 record from the Southeast Pacific, although the magnitude of δ^{13}C drop differs among these records (Figure S9a) and in some other cores is much less pronounced (Figure S9b). Given the rapidity of this transient benthic δ^{13}C event, previous authors attributed this positive δ^{13}C event to changes in ventilation and/or water mass structure driven by changes in winds or buoyancy forcing (Ronge et al., 2015; Sikes et al., 2016) in the SW Pacific. More specifically, during late HS1 when the Southern Hemisphere warmed, enhanced upwelling (Anderson et al., 2009) and a southward shift in the westerlies (Lamy et al., 2010; Putnam et al., 2010) and the sea ice edge (Ferrari et al., 2014; Rae et al., 2018) would have flushed respired carbon from these middepth waters (Jaccard et al., 2016; Rae et al., 2018) and/or supplied positive δ^{13}C to

these layers, due to enhanced air-sea gas exchange in the Southern Ocean. The reverse (i.e., reduced ventilation of intermediate waters) would have occurred during the Antarctic Cold Reversal (ACR), a period of SH cooling. A deepening (shoaling) of the AAIW/CDW boundary during late HS1 (ACR) may also contribute to this pattern (Figure S9).

However, there are also some differences in the nature of the deglacial benthic $\delta^{13}C$ signal from this region that may point to some added complexities (Figure S9b). For instance, some records are characterized by a more gradual increase in $\delta^{13}C$, ranging from 0.3–0.6‰ between 16.5 and 14 kyr BP, without any significant drop after HS1. It is possible that the temporal resolutions of some records (e.g., SO136-003 and SO213-84) are not high enough to capture the full $\delta^{13}C$ excursion. The potential influence of localized geological sources of CO_2 may also influence some of the records and introduce additional complexity to interpretation of benthic $\delta^{13}C$ records in this region. Direct observations of the $\delta^{13}C$ signature of the carbon coming from geological systems is crucial to improve our understanding of the benthic $\delta^{13}C$ from this region. A full investigation of benthic $\delta^{13}C$ records from intermediate depths is beyond the scope of the current study but has the potential to shed further light on these processes.

Notwithstanding the complexities described above, the large outgassing event between 16.5 and 14 kyr BP, documented by our new boron isotope data, was associated with a rapid increase in bottom water $[CO_3^{2-}]$, benthic $\delta^{13}C$ and $\Delta\Delta^{14}C$ increase, as well as high opal fluxes in the Southern Ocean, that would have accompanied release of respired—and possibly also geological—carbon from intermediate depths of the South Pacific, probably through a general enhancement of ocean ventilation relative to the glacial period. Taking our reconstructed ΔpCO_2 at face value, the data imply substantial carbon transfer from intermediate depths of the South Pacific to the upper ocean and eventually to the atmosphere between ~16.5 and 14 kyr BP.

4.2. Positive Air-Sea ΔpCO_2 Anomalies During the Deglaciation and Early Holocene

The median composite ΔpCO_2 curve shows a positive excursion of up to 50 ppm during the last deglaciation and more subtle positive excursions during the early Holocene (Figure 8e). Given the potential caveats of our new data, we also present a second composite that excludes the two records from Chatham Rise (Figure S10). Between 14–15 kyr BP and 5–10 kyr BP, ΔpCO_2 from the second composite is lower than the first one by ~10 ppm. However, excluding the two records from Chatham Rise in the composite does not change the first order picture–the composite ΔpCO_2 shows a positive anomaly over the last deglaciation and in the early Holocene, providing direct evidence that the ocean released carbon to the atmosphere at these times.

The deglacial ΔpCO_2 pulse is the most statistically significant, with the lower 2.5% quantile being above the equilibrium line (Figure 8e). This highlights the importance of ocean CO_2 outgassing for atmospheric pCO_2 rise during the last deglaciation. Although it is difficult to constrain how much area of the ocean each individual core represents, it appears that the deglacial ΔpCO_2 and presumably oceanic CO_2 outgassing flux encompassed a broader part of the global surface ocean than just the areas typically thought of as key for CO_2 outgassing. However, note that for each 1,000-year bin, there are roughly equal amounts of data from upwelling sites and nonupwelling sites (Figure 8f), whereas upwelling regions only occupy a relatively small amount of the global surface ocean area. These areas are connected to carbon in the deep and abyssal ocean and therefore were more likely to release extra carbon during the deglaciation. Interestingly, the site of PC75/83 and PS2498-1, both located in a moderate sink region today, appear to be a source of carbon over the last deglaciation, perhaps due to frontal shifts (Barker et al., 2009; Bostock et al., 2015) and/or stronger upwelling in the Southern Ocean (Anderson et al., 2009). Such transitions are not taken into account by correcting the location bias, but importantly, they are likely to reveal real signals of oceanic carbon cycle perturbations. Our results highlight a need to constrain the oceanic sink regions to better understand the complete history of air-sea CO_2 exchange over the last deglaciation.

ΔpCO_2 values in the late deglacial and early Holocene are also elevated, notably at a time of little change in atmospheric pCO_2. This may be explained if ocean CO_2 outgassing at this time is partially compensated by expansion of carbon sinks. The most likely candidate is regrowth of the terrestrial biosphere, which would also contribute to the increase in $\delta^{13}C$ in the deep ocean and the atmosphere at this time (Figure 8b). Thus, a substantial portion of the CO_2 released from the ocean during the late deglacial and early Holocene was probably being absorbed by terrestrial vegetation instead of remaining in the atmosphere,
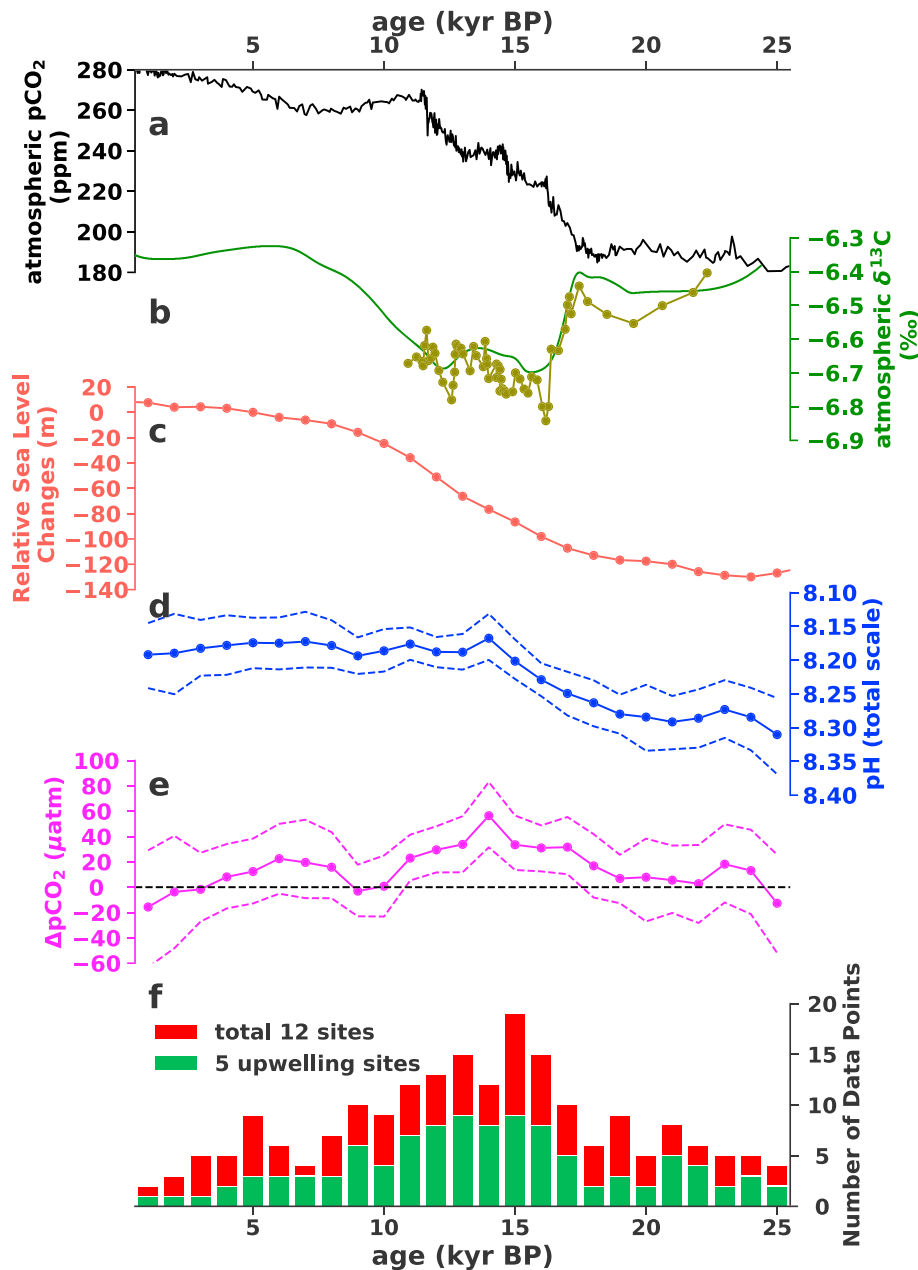
Figure 8. (a) Atmospheric pCO_2 (Bereiter et al., 2015); (b) $\delta^{13}C\text{-}CO_2$ from Schmitt et al. (2012; green) and Bauska et al. (2016; Olive); (c) relative sea level changes (Spratt & Lisiecki, 2016); (d) the median of 10,000 composite pH from 12 cores (thick blue line), the dotted lines represent 2.5% and 97.5% quantile, the black line with triangle markers represent the median of 10,000 composite pH without our two new records; (e) the median of 10,000 composite ΔpCO_2 from 12 cores (thick magenta line), the dotted lines represent 2.5% and 97.5% quantile; (f) number of data points from all (red bars)/upwelling (green bars) sites that go into each 1,000-year bin. Upwelling sites include ODP1238 from the eastern equatorial Pacific, PS2498 from the sub-Antarctic Atlantic, MD01-2416 from the subarctic Pacific, NIOP464 and AAS9 from the Northern Indian Ocean.

as previously suggested based on an increase in deep ocean carbonate ion concentration (Yu et al., 2010). There is also a significant peak in ΔpCO_2 in the mid Holocene, at a time of relatively stable $\delta^{13}C$ and gradually rising CO_2. This may be driven in part by CO_2 released from renewed shallow water $CaCO_3$ deposition (Ridgwell et al., 2003) as sea levels rose (Spratt & Lisiecki, 2016; Figure 8c), alongside carbonate compensation at depth (Broecker & Clark, 2007).

The interpretations presented here remain limited by a sparse sampling of the global ocean and age model uncertainties. Another caveat is the net exchange of carbon between the global ocean and the atmosphere depends not only on global mean ΔpCO_2 but also on the local CO_2 gas exchange rates governed by wind speed, which has not been quantitatively constrained here. Future work to increase the spatial and temporal resolution of planktic $\delta^{11}B$-based pH and CO_2 reconstructions, particularly in sink regions, and a better understanding of mechanisms responsible for the complex pattern of air-sea CO_2 exchange in different parts of the global Ocean, is essential to advancing our understanding of glacial/interglacial CO_2 variability.

5. Conclusions

We have added two new boron isotope records to the existing archive, partly filling an important spatial data gap in the subtropical-subpolar transition zone of the SW Pacific. Composite records of pH and pCO_2 were also compiled and reanalyzed from 12 sites that reveal intriguing patterns of ocean/atmosphere disequilibrium that may reflect a spatially and temporally complex history of CO_2 ventilation across the last 25 kyr. Based on results presented here we conclude the following:

1. New boron isotope-based pH records for the subtropical-subpolar South Pacific indicates the Chatham Rise was a source of carbon to the ocean/atmosphere during the last deglaciation. We suggest that respired carbon, and possibly geological carbon, from this region was ventilated through the Southern Ocean to the atmosphere between 16.5 and 14 kyr BP. However, there are mismatches in reconstructed pH/pCO_2 and SST between the two records that put a question mark on how representative these records are of wider oceanographic processes.
2. The composite pH derived from 12 boron isotope records throughout the global ocean agrees well with simulated GMSSpH by cGENIE and captures the first-order deglacial trend. The composite pCO_2 reveals pronounced ocean outgassing to the atmosphere from a broad part of the global surface ocean during the last deglaciation and early Holocene, although the sites included in the composite might be biased toward upwelling regions. Future work on reconstructing pCO_2 from sink regions is required to fully evaluate the dynamic history of air-sea exchange of CO_2. During the late deglaciation and early Holocene oceanic outgassing of CO_2 could partially be compensated by regrowth of terrestrial vegetation and carbonate compensation in the deep ocean.

References

Allen, K. A., Sikes, E. L., Hönisch, B., Elmore, A. C., Guilderson, T. P., Rosenthal, Y., & Anderson, R. F. (2015). Southwest Pacific deep water carbonate chemistry linked to high southern latitude climate and atmospheric CO_2 during the Last Glacial Termination. *Quaternary Science Reviews*, *122*, 180–191. https://doi.org/10.1016/j.quascirev.2015.05.007

Anderson, R. F., Ali, S., Bradtmiller, L. I., Nielsen, S. H. H., Fleisher, M. Q., Anderson, B. E., & Burckle, L. H. (2009). Wind-driven upwelling in the Southern Ocean and the deglacial rise in atmospheric CO_2. *Science*, *323*(5920), 1443–1448. https://doi.org/10.1126/science.1167441

Barker, S., Greaves, M., & Elderfield, H. (2003). A study of cleaning procedures used for foraminiferal Mg/Ca paleothermometry. *Geochemistry, Geophysics, Geosystems*, *4*(9), 8407. https://doi.org/10.1029/2003GC000559

Barker, S., Diz, P., Vautravers, M. J., Pike, J., Knorr, G., Hall, I. R., & Broecker, W. S. (2009). Interhemispheric Atlantic seesaw response during the last deglaciation. *Nature*, *457*(7233), 1097–1102. https://doi.org/10.1038/nature07770

Basak, C., Fröllje, H., Lamy, F., Gersonde, R., Benz, V., Anderson, R. F., et al. (2018). Breakup of last glacial deep stratification in the South Pacific. *Science*, *359*(6378), 900–904. https://doi.org/10.1126/science.aao2473

Bauska, T. K., Baggenstos, D., Brook, E. J., Mix, A. C., Marcott, S. A., Petrenko, V. V., et al. (2016). Carbon isotopes characterize rapid changes in atmospheric carbon dioxide during the last deglaciation. *Proceedings of the National Academy of Sciences*, *113*(13), 3465–3470. https://doi.org/10.1073/pnas.1513868113

Bereiter, B., Eggleston, S., Schmitt, J., Nehrbass-Ahles, C., Stocker, T. F., Fischer, H., et al. (2015). Revision of the EPICA Dome C CO_2 record from 800 to 600 kyr before present: Analytical bias in the EDC CO_2 record. *Geophysical Research Letters*, *42*, 542–549. https://doi.org/10.1002/2014GL061957

Bostock, H. C., Hayward, B. W., Neil, H. L., Sabaa, A. T., & Scott, G. H. (2015). Changes in the position of the subtropical front south of New Zealand since the last glacial period. *Paleoceanography*, *30*, 824–844. https://doi.org/10.1002/2014PA002652

Broecker, W., & Clark, E. (2007). Is the magnitude of the carbonate ion decrease in the abyssal ocean over the last 8 kyr consistent with the 20 ppm rise in atmospheric CO_2 content?: Holocene decrease in deep-sea carbonate. *Paleoceanography*, *22*, PA1202. https://doi.org/10.1029/2006PA001311

Cao, L., Eby, M., Ridgwell, A., Caldeira, K., Archer, D., Ishida, A., et al. (2009). The role of ocean transport in the uptake of anthropogenic CO_2. *Biogeosciences*, *6*(3), 375–390. https://doi.org/10.5194/bg-6-375-2009

Chase, Z., Anderson, R. F., Fleisher, M. Q., & Kubik, P. W. (2003). Accumulation of biogenic and lithogenic material in the Pacific sector of the Southern Ocean during the past 40,000 years. *Deep Sea Research Part II: Topical Studies in Oceanography*, *50*(3–4), 799–832. https://doi.org/10.1016/S0967-0645(02)00595-7

Coffin, R. B., Boyd, T. J., Rose, P. S., Yoza, B., Millholland, L. C., Downer, R., & Woods, S. (2013). Geochemical cruise report SO226/2 RV Sonne Chatham Rise Expedition: Fort Belvoir, VA: Defense Technical Information Center. https://doi.org/10.21236/ADA587416

Davy, B., Pecher, I., Wood, R., Carter, L., & Gohl, K. (2010). Gas escape features off New Zealand: Evidence of massive release of methane from hydrates: MASSIVE NZ GAS ESCAPE FEATURES. *Geophysical Research Letters*, *37*, L21309. https://doi.org/10.1029/2010GL045184

Dickson, A. G. (1990). Thermodynamics of the dissociation of boric acid in synthetic seawater from 273.15 to 318.15 K. *Deep Sea Research Part A. Oceanographic Research Papers*, *37*(5), 755–766. https://doi.org/10.1016/0198-0149(90)90004-F

Edgar, K. M., Anagnostou, E., Pearson, P. N., & Foster, G. L. (2015). Assessing the impact of diagenesis on $\delta^{11}B$, $\delta^{13}C$, $\delta^{18}O$, Sr/Ca and B/Ca values in fossil planktic foraminiferal calcite. *Geochimica et Cosmochimica Acta*, *166*, 189–209. https://doi.org/10.1016/j.gca.2015.06.018

Edwards, N. R., & Marsh, R. (2005). Uncertainties due to transport-parameter sensitivity in an efficient 3-D ocean-climate model. *Climate Dynamics*, *24*(4), 415–433. https://doi.org/10.1007/s00382-004-0508-8

Evans, D., Wade, B. S., Henehan, M., Erez, J., & Müller, W. (2016). Revisiting carbonate chemistry controls on planktic foraminifera Mg/Ca: Implications for sea surface temperature and hydrology shifts over the Paleocene–Eocene Thermal Maximum and Eocene–Oligocene transition. *Climate of the Past*, *12*(4), 819–835. https://doi.org/10.5194/cp-12-819-2016

Ezat, M. M., Rasmussen, T. L., Hönisch, B., Groeneveld, J., & deMenocal, P. (2017). Episodic release of CO_2 from the high-latitude North Atlantic Ocean during the last 135 kyr. *Nature Communications*, *8*, 14498. https://doi.org/10.1038/ncomms14498

Farmer, J. R., Hönisch, B., & Uchikawa, J. (2016). Single laboratory comparison of MC-ICP-MS and N-TIMS boron isotope analyses in marine carbonates. *Chemical Geology*, *447*, 173–182. https://doi.org/10.1016/j.chemgeo.2016.11.008

Ferrari, R., Jansen, M. F., Adkins, J. F., Burke, A., Stewart, A. L., & Thompson, A. F. (2014). Antarctic sea ice control on ocean circulation in present and glacial climates. *Proceedings of the National Academy of Sciences*, *111*(24), 8753–8758. https://doi.org/10.1073/pnas.1323922111

Foster, G. L. (2008). Seawater pH, pCO$_2$ and $[CO^{2-}_3]$ variations in the Caribbean Sea over the last 130 kyr: A boron isotope and B/Ca study of planktic foraminifera. *Earth and Planetary Science Letters*, *271*(1–4), 254–266. https://doi.org/10.1016/j.epsl.2008.04.015

Foster, G. L., & Sexton, P. F. (2014). Enhanced carbon dioxide outgassing from the eastern equatorial Atlantic during the last glacial. *Geology*, *42*(11), 1003–1006. https://doi.org/10.1130/G35806.1

Foster, G. L., Hönisch, B., Paris, G., Dwyer, G. S., Rae, J. W. B., Elliott, T., et al. (2013). Interlaboratory comparison of boron isotope analyses of boric acid, seawater and marine $CaCO_3$ by MC-ICPMS and NTIMS. *Chemical Geology*, *358*, 1–14. https://doi.org/10.1016/j.chemgeo.2013.08.027

Foster, G. L. & Rae, J. W. B. (2016). Reconstructing ocean pH with boron isotopes in foraminifera. *Annual Review of Earth and Planetary Sciences*, *44*(1), 207–237. https://doi.org/10.1146/annurev-earth-060115-012226

Franois, R., Altabet, M. A., Yu, E.-F., Sigman, D. M., Bacon, M. P., Frank, M., et al. (1997). Contribution of Southern Ocean surface-water stratification to low atmospheric CO_2 concentrations during the last glacial period. *Nature*, *389*(6654), 929–935. https://doi.org/10.1038/40073

Fry, C. H., Tyrrell, T., Hain, M. P., Bates, N. R., & Achterberg, E. P. (2015). Analysis of global surface ocean alkalinity to determine controlling processes. *Marine Chemistry*, *174*, 46–57. https://doi.org/10.1016/j.marchem.2015.05.003

Gray, W. R., & Evans, D. (2019). Non-thermal influences on Mg/Ca in planktonic foraminifera: A review of culture studies and application to the last glacial maximum. *Paleoceanography and Paleoclimatology*, *34*, 306–315. https://doi.org/10.1029/2018PA003517

Gray, W. R., Rae, J. W. B., Wills, R. C. J., Shevenell, A. E., Taylor, B., Burke, A., et al. (2018). Deglacial upwelling, productivity and CO_2 outgassing in the North Pacific Ocean. *Nature Geoscience*, *11*(5), 340–344. https://doi.org/10.1038/s41561-018-0108-6

Gray, W. R., Weldeab, S., Lea, D. W., Rosenthal, Y., Gruber, N., Donner, B., & Fischer, G. (2018). The effects of temperature, salinity, and the carbonate system on Mg/Ca in Globigerinoides ruber (white): A global sediment trap calibration. *Earth and Planetary Science Letters*, *482*, 607–620. https://doi.org/10.1016/j.epsl.2017.11.026

Hain, M. P., Sigman, D. M., & Haug, G. H. (2010). Carbon dioxide effects of Antarctic stratification, North Atlantic Intermediate Water formation, and sub-Antarctic nutrient drawdown during the last ice age: Diagnosis and synthesis in a geochemical box model: Atmospheric CO $_2$ during the last ice age. *Global Biogeochemical Cycles*, *24*, GB4023. https://doi.org/10.1029/2010GB003790

Haslett, J., & Parnell, A. (2008). A simple monotone process with application to radiocarbon-dated depth chronologies. *Journal of the Royal Statistical Society: Series C: Applied Statistics*, *57*(4), 399–418. https://doi.org/10.1111/j.1467-9876.2008.00623.x

Hemming, N. G., & Hanson, G. N. (1992). Boron isotopic composition and concentration in modern marine carbonates. *Geochimica et Cosmochimica Acta*, *56*(1), 537–543. https://doi.org/10.1016/0016-7037(92)90151-8

Henehan, M. J., Foster, G. L., Bostock, H. C., Greenop, R., Marshall, B. J., & Wilson, P. A. (2016). A new boron isotope-pH calibration for Orbulina universa, with implications for understanding and accounting for 'vital effects'. *Earth and Planetary Science Letters*, *454*, 282–292. https://doi.org/10.1016/j.epsl.2016.09.024

Henehan, M. J., Rae, J. W. B., Foster, G. L., Erez, J., Prentice, K. C., Kucera, M., et al. (2013). Calibration of the boron isotope proxy in the planktonic foraminifera Globigerinoides ruber for use in palaeo-CO_2 reconstruction. *Earth and Planetary Science Letters*, *364*, 111–122. https://doi.org/10.1016/j.epsl.2012.12.029

Hines, S. K. V., Southon, J. R., & Adkins, J. F. (2015). A high-resolution record of Southern Ocean intermediate water radiocarbon over the past 30,000 years. *Earth and Planetary Science Letters*, *432*, 46–58. https://doi.org/10.1016/j.epsl.2015.09.038

Hönisch, B., Bijma, J., Russell, A. D., Spero, H. J., Palmer, M. R., Zeebe, R. E., & Eisenhauer, A. (2003). The influence of symbiont photosynthesis on the boron isotopic composition of foraminifera shells. *Marine Micropaleontology*, *49*(1–2), 87–96. https://doi.org/10.1016/S0377-8398(03)00030-6

Hönisch, B., & Hemming, N. G. (2005). Surface ocean pH response to variations in pCO2 through two full glacial cycles. *Earth and Planetary Science Letters*, *236*(1–2), 305–314. https://doi.org/10.1016/j.epsl.2005.04.027

Jaccard, S. L., Galbraith, E. D., Martínez-García, A., & Anderson, R. F. (2016). Covariation of deep Southern Ocean oxygenation and atmospheric CO_2 through the last ice age. *Nature*, *530*(7589), 207–210. https://doi.org/10.1038/nature16514

Jonkers, L., & Kučera, M. (2015). Global analysis of seasonality in the shell flux of extant planktonic foraminifera. *Biogeosciences*, *12*(7), 2207–2226. https://doi.org/10.5194/bg-12-2207-2015

Kısakürek, B., Eisenhauer, A., Böhm, F., Garbe-Schönberg, D., & Erez, J. (2008). Controls on shell Mg/Ca and Sr/Ca in cultured planktonic foraminiferan, *Globigerinoides ruber* (white). *Earth and Planetary Science Letters*, *273*(3–4), 260–269. https://doi.org/10.1016/j.epsl.2008.06.026

Klochko, K., Kaufman, A. J., Yao, W., Byrne, R. H., & Tossell, J. A. (2006). Experimental measurement of boron isotope fractionation in seawater. *Earth and Planetary Science Letters*, *248*(1–2), 276–285. https://doi.org/10.1016/j.epsl.2006.05.034

Lamy, F., Kilian, R., Arz, H. W., Francois, J.-P., Kaiser, J., Prange, M., & Steinke, T. (2010). Holocene changes in the position and intensity of the southern westerly wind belt. *Nature Geoscience*, *3*(10), 695–699. https://doi.org/10.1038/ngeo959

Lauvset, S. K., Key, R. M., Olsen, A., van Heuven, S., Velo, A., Lin, X., et al. (2016). A new global interior ocean mapped climatology: the 1° × 1° GLODAP version 2. *Earth System Science Data*, *8*, 325–340. https://doi.org/10.5194/essd-8-325-2016

Lea, D. W., Mashiotta, T. A., & Spero, H. J. (1999). Controls on magnesium and strontium uptake in planktonic foraminifera determined by live culturing. *Geochimica et Cosmochimica Acta*, *63*(16), 2369–2379. https://doi.org/10.1016/S0016-7037(99)00197-0

Lowe, D. J., Blaauw, M., Hogg, A. G., & Newnham, R. M. (2013). Ages of 24 widespread tephras erupted since 30,000 years ago in New Zealand, with re-evaluation of the timing and palaeoclimatic implications of the Lateglacial cool episode recorded at Kaipo bog. *Quaternary Science Reviews*, *74*, 170–194. https://doi.org/10.1016/j.quascirev.2012.11.022

Lund, D. C., Asimow, P. D., Farley, K. A., Rooney, T. O., Seeley, E., Jackson, E. W., & Durham, Z. M. (2016). Enhanced East Pacific Rise hydrothermal activity during the last two glacial terminations. *Science*, *351*(6272), 478–482. https://doi.org/10.1126/science.aad4296

Marcott, S. A., Bauska, T. K., Buizert, C., Steig, E. J., Rosen, J. L., Cuffey, K. M., et al. (2014). Centennial-scale changes in the global carbon cycle during the last deglaciation. *Nature*, *514*(7524), 616–619. https://doi.org/10.1038/nature13799

Martínez-Botí, M. A., Marino, G., Foster, G. L., Ziveri, P., Henehan, M. J., Rae, J. W. B., et al. (2015). Boron isotope evidence for oceanic carbon dioxide leakage during the last deglaciation. *Nature*, *518*(7538), 219–222. https://doi.org/10.1038/nature14155

Martinez-Garcia, A., Sigman, D. M., Ren, H., Anderson, R. F., Straub, M., Hodell, D. A., et al. (2014). Iron Fertilization of the Subantarctic Ocean during the Last Ice Age. *Science*, *343*(6177), 1347–1350. https://doi.org/10.1126/science.1246848

McCave, I. N., Carter, L., & Hall, I. R. (2008). Glacial–interglacial changes in water mass structure and flow in the SW Pacific Ocean. *Quaternary Science Reviews*, *27*(19–20), 1886–1908. https://doi.org/10.1016/j.quascirev.2008.07.010

Monnin, E., Indermuhle, A., Dallenbach, A., Fluckiger, J., Stauffer, B., Stocker, T. F., et al. (2001). Atmospheric CO_2 concentrations over the Last Glacial termination. *Science*, *291*(5501), 112–114. https://doi.org/10.1126/science.291.5501.112

Naik, S. S., Divakar Naidu, P., Foster, G. L., & Martínez-Botí, M. A. (2015). Tracing the strength of the southwest monsoon using boron isotopes in the eastern Arabian Sea. *Geophysical Research Letters*, *42*, 1450–1458. https://doi.org/10.1002/2015GL063089

Palmer, M. R., Brummer, G. J., Cooper, M. J., Elderfield, H., Greaves, M. J., Reichart, G. J., et al. (2010). Multi-proxy reconstruction of surface water pCO_2 in the northern Arabian Sea since 29 ka. *Earth and Planetary Science Letters*, *295*(1–2), 49–57. https://doi.org/10.1016/j.epsl.2010.03.023

Palmer, M. R., & Pearson, P. N. (2003). A 23,000-year record of surface water pH and pCO_2 in the Western Equatorial Pacific Ocean. *Science*, *300*(5618), 480–482. https://doi.org/10.1126/science.1080796

Petit, J. R., Jouzel, J., Raynaud, D., Barkov, N. I., Delaygue, G., Delmotte, M., et al. (1999). Climate and atmospheric history of the past 420,000 years from the Vostok ice core, Antarctica. *Nature*, *399*, 429–436.

Putnam, A. E., Denton, G. H., Schaefer, J. M., Barrell, D. J. A., Andersen, B. G., Finkel, R. C., et al. (2010). Glacier advance in southern middle-latitudes during the Antarctic Cold Reversal. *Nature Geoscience*, *3*(10), 700–704. https://doi.org/10.1038/ngeo962

Rae, J. W. B., Burke, A., Robinson, L. F., Adkins, J. F., Chen, T., Cole, C., et al. (2018). CO_2 storage and release in the deep Southern Ocean on millennial to centennial timescales. *Nature*, *562*(7728), 569–573. https://doi.org/10.1038/s41586-018-0614-0

Rae, J. W. B. (2018). Boron isotopes in foraminifera: systematics, biomineralisation, and CO_2 reconstruction. In H. Marschall & G. Foster (Eds.), *Boron isotopes: The fifth element* (pp. 107–143). Cham: Springer International Publishing. https://doi.org/10.1007/978-3-319-64666-4_5

Rae, J. W. B., Foster, G. L., Schmidt, D. N., & Elliott, T. (2011). Boron isotopes and B/Ca in benthic foraminifera: Proxies for the deep ocean carbonate system. *Earth and Planetary Science Letters*, *302*(3–4), 403–413. https://doi.org/10.1016/j.epsl.2010.12.034

Raitzsch, M., Bijma, J., Benthien, A., Richter, K.-U., Steinhoefel, G., & Kučera, M. (2018). Boron isotope-based seasonal paleo-pH reconstruction for the Southeast Atlantic—A multispecies approach using habitat preference of planktonic foraminifera. *Earth and Planetary Science Letters*, *487*, 138–150. https://doi.org/10.1016/j.epsl.2018.02.002

Regenberg, M., Regenberg, A., Garbe-Schönberg, D., & Lea, D. W. (2014). Global dissolution effects on planktonic foraminiferal Mg/Ca ratios controlled by the calcite-saturation state of bottom waters. *Paleoceanography*, *29*, 127–142. https://doi.org/10.1002/2013PA002492

Reimer, P. J., Bard, E., Bayliss, A., Beck, J. W., Blackwell, P. G., Ramsey, C. B., et al. (2013). IntCal13 and Maine13 radiocarbon age calibration curves 0-50000 years cal BP. *Radiocarbon*, *55*(4), 1869–1887. https://doi.org/10.2458/azu_js_rc.55.16947

Ridgwell, A., Hargreaves, J. C., Edwards, N. R., Annan, J. D., Lenton, T. M., Marsh, R., et al. (2007). Marine geochemical data assimilation in an efficient Earth System Model of global biogeochemical cycling. *Biogeosciences*, *4*(1), 87–104. https://doi.org/10.5194/bg-4-87-2007

Ridgwell, A. J., Watson, A. J., Maslin, M. A., & Kaplan, J. O. (2003). Implications of coral reef buildup for the controls on atmospheric CO_2 since the Last Glacial Maximum. *Paleoceanography*, *18*(4), 1083. https://doi.org/10.1029/2003PA000893

Ronge, T. A., Tiedemann, R., Lamy, F., Köhler, P., Alloway, B. V., De Pol-Holz, R., et al. (2016). Radiocarbon constraints on the extent and evolution of the South Pacific glacial carbon pool. *Nature Communications*, *7*, 11487. https://doi.org/10.1038/ncomms11487

Ronge, T. A., Steph, S., Tiedemann, R., Prange, M., Merkel, U., Nürnberg, D., & Kuhn, G. (2015). Pushing the boundaries: Glacial/interglacial variability of intermediate and deep waters in the southwest Pacific over the last 350,000 years: Variability in SW-Pacific AAIW and UCDW. *Paleoceanography*, *30*, 23–38. https://doi.org/10.1002/2014PA002727

Russell, A. D., Hönisch, B., Spero, H. J., & Lea, D. W. (2004). Effects of seawater carbonate ion concentration and temperature on shell U, Mg, and Sr in cultured planktonic foraminifera. *Geochimica et Cosmochimica Acta*, *68*(21), 4347–4361. https://doi.org/10.1016/j.gca.2004.03.013

Sanyal, A., Bijma, J., Spero, H., & Lea, D. W. (2001). Empirical relationship between pH and the boron isotopic composition of *Globigerinoides sacculifer*: Implications for the boron isotope paleo-pH proxy. *Paleoceanography*, *16*(5), 515–519. https://doi.org/10.1029/2000PA000547

Sanyal, A., Hemming, N. G., Broecker, W. S., Lea, D. W., Spero, H. J., & Hanson, G. N. (1996). Oceanic pH control on the boron isotopic composition of foraminifera: Evidence from culture experiments. *Paleoceanography*, *11*(5), 513–517. https://doi.org/10.1029/96PA01858

Schmitt, J., Schneider, R., Elsig, J., Leuenberger, D., Lourantou, A., Chappellaz, J., et al. (2012). Carbon Isotope Constraints on the Deglacial CO_2 Risefrom Ice Cores. *Science*, *336*(6082), 711–714. https://doi.org/10.1126/science.1217161

Sikes, E. L., Elmore, A. C., Allen, K. A., Cook, M. S., & Guilderson, T. P. (2016). Glacial water mass structure and rapid $\delta^{18}O$ and $\delta^{13}C$ changes during the last glacial termination in the Southwest Pacific. *Earth and Planetary Science Letters*, *456*, 87–97. https://doi.org/10.1016/j.epsl.2016.09.043

Sikes, E. L., & Guilderson, T. P. (2016). Southwest Pacific Ocean surface reservoir ages since the last glaciation: Circulation insights from multiple-core studies. *Paleoceanography*, *31*, 298–310. https://doi.org/10.1002/2015PA002855

Sikes, E. L., Samson, C. R., Guilderson, T. P., & Howard, W. R. (2000). Old radiocarbon ages in the southwest Pacific Ocean during the last glacial period and deglaciation. *Nature*, *405*, 555–559.

Skinner, L., McCave, I. N., Carter, L., Fallon, S., Scrivner, A. E., & Primeau, F. (2015). Reduced ventilation and enhanced magnitude of the deep Pacific carbon pool during the last glacial period. *Earth and Planetary Science Letters*, *411*, 45–52. https://doi.org/10.1016/j.epsl.2014.11.024

Spratt, R. M., & Lisiecki, L. E. (2016). A Late Pleistocene sea level stack. *Climate of the Past*, *12*(4), 1079–1092. https://doi.org/10.5194/cp-12-1079-2016

Stern, J. V., & Lisiecki, L. E. (2014). Termination 1 timing in radiocarbon-dated regional benthic δ^{18}O stacks. *Paleoceanography*, *29*, 1127–1142. https://doi.org/10.1002/2014PA002700

Stott, L., & Timmermann, A. (2011). Hypothesized link between glacial/interglacial atmospheric CO_2 cycles and storage/release of CO2-rich fluids from deep-sea sediments. In H. Rashid, L. Polyak, & E. Mosley-Thompson (Eds.), *Abrupt climate change: Mechanisms, patterns, and impacts*, *Geophysical Monograph Series* (Vol. 193, pp. 123–138). Washington, DC: American Geophysical Union. https://doi.org/10.1029/2010GM001052

Studer, A. S., Sigman, D. M., Martínez-García, A., Benz, V., Winckler, G., Kuhn, G., et al. (2015). Antarctic Zone nutrient conditions during the last two glacial cycles: Antarctic zone nutrient conditions. *Paleoceanography*, *30*, 845–862. https://doi.org/10.1002/2014PA002745

Takahashi, T., Sutherland, S. C., Wanninkhof, R., Sweeney, C., Feely, R. A., Chipman, D. W., et al. (2009). Climatological mean and decadal change in surface ocean pCO$_2$, and net sea–air CO_2 flux over the global oceans. *Deep Sea Research Part II: Topical Studies in Oceanography*, *56*(8–10), 554–577. https://doi.org/10.1016/j.dsr2.2008.12.009

Taylor, B. J., Rae, J. W. B., Gray, W. R., Darling, K. F., Burke, A., Gersonde, R., et al. (2018). Distribution and ecology of planktic foraminifera in the North Pacific: Implications for paleo-reconstructions. *Quaternary Science Reviews*, *191*, 256–274. https://doi.org/10.1016/j.quascirev.2018.05.006

Toggweiler, J. R. (1999). Variation of atmospheric CO_2 by ventilation of the ocean's deepest water. *Paleoceanography*, *14*(5), 571–588. https://doi.org/10.1029/1999PA900033

Vogl, J., & Rosner, M. (2012). Production and certification of a unique set of isotope and delta reference materials for boron isotope determination in geochemical, environmental and industrial materials. *Geostandards and Geoanalytical Research*, *36*(2), 161–175. https://doi.org/10.1111/j.1751-908X.2011.00136.x

Yu, J., Broecker, W. S., Elderfield, H., Jin, Z., McManus, J., & Zhang, F. (2010). Loss of Carbon from the Deep Sea Since the Last Glacial Maximum. *Science*, *330*(6007), 1084–1087. https://doi.org/10.1126/science.1193221

Yu, J., Thornalley, D. J. R., Rae, J. W. B., & McCave, N. I. (2013). Calibration and application of B/Ca, Cd/Ca, and δ^{11}B in *Neogloboquadrina pachyderma* (sinistral) to constrain CO_2 uptake in the subpolar North Atlantic during the last deglaciation. *Paleoceanography*, *28*, 237–252. https://doi.org/10.1002/palo.20024

Zeebe, R. E., Wolf-Gladrow, D. A., Bijma, J., & Hönisch, B. (2003). Vital effects in foraminifera do not compromise the use of δ^{11}B as a paleo-pH indicator: Evidence from modeling: Cretaceous marine temperature evolution. *Paleoceanography*, *18*(2), 1043. https://doi.org/10.1029/2003PA000881